Atmos. Chem. Phys., 9, 3755–3776, 2009
www.atmos-chem-phys.net/9/3755/2009/


Atmospheric Chemistry and Physics

# Synoptic influences on springtime tropospheric $O_3$ and CO over the North American export region observed by TES

**J. Hegarty, H. Mao, and R. Talbot**

Institute for the Study of Earth, Oceans and Space, Climate Change Research Center, University of New Hampshire, Durham, New Hampshire 03824, USA

Received: 27 August 2008 – Published in Atmos. Chem. Phys. Discuss.: 19 November 2008
Revised: 25 May 2009 – Accepted: 25 May 2009 – Published: 11 June 2009

**Abstract.** The relationship between synoptic circulation patterns over the western North Atlantic Ocean in spring (March, April, and May) and tropospheric $O_3$ and CO was investigated using retrievals from the Tropospheric Emission Spectrometer (TES) for 2005 and 2006. Seasonal composites of TES retrievals reprocessed to remove the artificial geographic structure added from the a priori revealed a channel of slightly elevated $O_3$ (>55 ppbv) and CO (>115 ppbv) at the 681 hPa retrieval level between 30° N and 45° N extending from North America out over the Atlantic Ocean. Ozone and CO in this region were correlated at $r$=0.22 with a slope value of 0.13 mol mol$^{-1}$ indicative of the overall impact of photochemical chemical processes in North American continental export. Composites of TES retrievals for the six predominant circulation patterns identified as map types from sea level pressure fields of the NCEP FNL analyses showed large variability in the distribution of tropospheric $O_3$. Map types MAM2 and MAM3 featuring cyclones near the US east coast produced the greatest export to the lower free troposphere with $O_3$>65 ppbv and a relatively well-defined $O_3$-CO correlation (slope values near 0.20 mol mol$^{-1}$). The ensembles of HYSPLIT backward trajectories indicated that the high $O_3$ levels were possibly a result of pollutants lofted to the free troposphere by the warm conveyor belt (WCB) of a cyclone. An important finding was that pollutant export occurred in the main WCB branch to the east of the cyclone and in a secondary branch circling to the back of the cyclone center. Conversely, a map type featuring a large anticyclone dominating the flow over the US east coast (MAM6) restricted export with $O_3$ levels generally <55 ppbv and CO levels generally <110 ppbv. There was also evidence of stratospheric intrusions particularly to the north of 45° N in the 316 hPa composites predominately for MAM1 which featured a large cyclone near Newfoundland. However, the concurrence of these intrusions with pollutant export, specifically in the southwestern North Atlantic Ocean, made it difficult to delineate their respective contributions to the 681 hPa $O_3$ composites.

*Correspondence to:* J. Hegarty
(jhegarty@ccrc.sr.unh.edu)

## 1 Introduction

An important and ongoing area of research is the quantification of air pollutant outflow from North America and identification of the meteorological processes that govern the continental export. North American outflow can travel from within the continental boundary layer to the North Atlantic Ocean by low-level westerly winds, and portions of these plumes may be incorporated into the marine free troposphere because of the difference in continental and marine boundary layer structure (Angevine et al., 2004; Rodrigues et al., 2004). This scenario enables $O_3$ to be slowly transported across the Atlantic Ocean (∼10 days transport times in summer months) at low levels (2–4 km) but cut-off from the destructive (halogen) chemistry of the MBL (Owen et al., 2006). Pollutants may also be transported from the continental boundary layer in a warm conveyor belt (WCB) of a synoptic-scale mid-latitude cyclone into streams of fast moving middle and upper tropospheric westerly winds (Eckhardt et al., 2004; Crielson et al., 2003; Stohl et al., 2003a). Some WCBs originating over North America can transport $O_3$ and precursors to the free troposphere over Europe within 4–5 days (Stohl et al., 1999, 2003a) where descending motions carry them back toward the surface causing ground-level $O_3$ mixing ratios to rise, but so far this has only been observed at high elevation sites in the Alps (Huntrieser et al., 2005). However, the same cyclones responsible for lofting $O_3$-forming anthropogenic pollutants from the continental boundary layer to the free troposphere may also mix down $O_3$ of stratospheric origin, which inevitably complicates the

quantification of the tropospheric $O_3$ budgets (Cooper et al., 2001, 2002; Moody et al, 1996; Merrill et al., 1996; Oltmans et al., 1996; Polvani and Esler, 2007). Thus information on the 3-dimensional distribution of $O_3$ and its precursors as well as the air mass transport history are required to ascertain the contributions of the various sources to observed $O_3$ levels.

A number of field missions (e.g., NARE, NEAQS2002, and INTEXA/ICARTT2004) have been dedicated to understanding the composition of North American outflow (e.g., Parrish et al., 1993, 1998; Banic et al. 1996; Berkowitz et al., 1996; Cooper et al., 2001, 2002, 2005; Fehsenfeld et al., 2006; Singh et al., 2006; Mao et al., 2006). In many of these studies critical vertical information was obtained via highly coordinated measurement programs involving ozonesonde networks, ships and aircraft. However, these observations were only feasible for short intensive study periods over limited areas and were sparse in overall density. Therefore long-term continuous measurements over extensive areas are highly desirable to fill this critical data gap.

A few modeling studies have complimented the field campaigns by examining 3-dimensional distributions of $O_3$ over the North Atlantic and Europe as a result of North American outflow for extended periods (Kasibhatla et al., 1996; Jacob et al., 1993; Li et al., 2005; Auvray and Bey, 2005). However, uncertainties in emissions profiles, the lack of observations for the initialization of chemical fields, and the inherent uncertainties in the modeling of atmospheric circulations and chemical processes present significant challenges in interpretation of the results (Auvray et al., 2007).

The tropospheric ozone ($O_3$) column abundance sheds insight on the influence of anthropogenic activities on the global atmospheric composition. For decades the tropospheric $O_3$ column was estimated based on the satellite measurements of the total column and the stratospheric profile due to lack of tropospheric vertical profiles (Fishman et al., 1990, 2005; Creilson et al., 2003; Stohl et al., 2003a). These estimates were highly uncertain, and it was difficult to obtain an understanding of vertical transport of surface pollutants and stratospheric intrusions.

The launch of EOS-AURA on 15 July 2004 with the Tropospheric Emission Spectrometer (TES) onboard, enabled for the first time quantification of the tropospheric column and profile of $O_3$. TES is a Fourier transform infrared spectrometer designed to measure global distributions of tropospheric $O_3$ and its precursors such as carbon monoxide (CO) (Beer et al., 2001). These measurements may prove to be crucial for the study of many global air quality problems, including the estimation of intercontinental transport (ICT) of pollutants exported from North America.

The ultimate application of TES measurements is to help address some of these challenges by providing a continuous independent 3-dimensional observational data base for comparison with other observations and model simulations, and to improve model performance through data assimilation techniques. However, they must first be thoroughly examined and evaluated for accuracy and information content. Such efforts are currently ongoing and have included the statistical validation of TES $O_3$ profiles against global sets of ozonesondes (Worden et al., 2007; Nassar et al., 2008) and comparisons with aircraft and ground-based measurements over the highly polluted regions such as Mexico City (Shim et al., 2007). Zhang et al. (2006) have examined North American export and found a positive correlation between lower-middle tropospheric TES $O_3$ and CO downwind of the US for July 2005. However, a yet unexplored critical issue to the study of North American export is what these measurements suggest corresponding to the highly variable circulation patterns that affect the continental east coast and in particular the northeastern US and adjacent Atlantic Ocean. In this study we aimed to identify and examine any discernable associations between the variability in $O_3$ and CO captured in TES observations and springtime synoptic-scale atmospheric circulations which regulate transport and dispersion of pollutants in the North American export region.

Tropospheric $O_3$ levels in many locations in the Northern Hemisphere show a distinct seasonal variation with levels peaking in spring and remaining high during the summer months (Monks, 2000). However, the frequency of mid-latitude cyclones and anticyclones decreases in summertime and circulation over the eastern US and western North Atlantic tends to be dominated by the large persistent subtropical Bermuda/Azores High (Ziska and Smith, 1980; Bell and Bosart, 1989; Serreze et al., 1997; Key and Chan, 1999; Owen et al., 2006). Therefore, in this study we focused on the spring, i.e., March, April, and May (MAM), and classified the TES retrievals for the 2005 and 2006 seasons by circulation type over a domain covering the eastern US, southeastern Canada and the adjacent western North Atlantic Ocean.

## 2 Data and methods

### 2.1 TES data

Aura is in near polar, sun-synchronous orbit around the Earth with an ascending equatorial crossing at approximately 13:45 local time (Schoeberl et al., 2006) (http://aura.gsfc.nasa.gov). Onboard Aura, TES scans the atmosphere in the infrared to measure $O_3$ and $O_3$ precursors such as CO. TES produces a 16-orbit Global Survey every other day while the alternate days are reserved for special observations over selected parts of the globe. For this study we used the TES Level 2 V002 Global Survey data (Osterman et al., 2007a) during MAM of 2005 and 2006. The nadir on-the-ground footprint is approximately 5.3 km × 8.4 km (Bowman et al., 2002; Beer et al., 2001, 2006). The along-orbit spacing between footprints for the Global Survey runs was approximately 544 km before 25 May 2005 but improved to

approximately 182 km after the limb scans were eliminated and replaced by an additional nadir scan (Osterman et al., 2007b). Each orbit was approximately 22° longitude apart. TES vertical coverage extends from 0–∼33 km and in cloud-free conditions the vertical resolution is approximately 6 km with sensitivity to both the lower and upper troposphere as well as the stratosphere (Bowman et al., 2002; Worden et al., 2004).

Atmospheric parameters are retrieved from the measured TES radiances using algorithms described by Rodgers (2000), Worden et al. (2004) and Bowman et al. (2002, 2006). The retrieved vertical profiles can be related to the true profiles and a priori constraint profiles with the relationship:

$$\hat{x} = x_c + A(x - x_c) \quad (1)$$

The vectors $\hat{x}$,$x$ and $x_c$ represent the retrieved, true and a priori constraint profiles, respectively. Since the measured TES radiances are affected by a significant vertical extent of the atmosphere, the true state at any given atmospheric level can influence the retrieved state values at many adjacent levels. The averaging kernel matrix $\boldsymbol{A}$ defines the contribution of each element of the true state vector to the retrieval at a particular pressure (or altitude) level. For example, the averaging kernel for a retrieved profile near 31° N and 74° W on 6 April 2006 indicated that the 681 hPa $O_3$ estimate was affected by the true state $O_3$ profile not only at 681 hPa but from all levels between approximately 900 and 450 hPa (Fig. 1). This vertical smoothing effect which varies from profile to profile based on the meteorological parameters such as temperature humidity and cloud cover as well as the vertical distribution of $O_3$ or CO must be factored into any interpretation of the TES measurements.

A weakness of TES is its general inability to accurately measure boundary layer parameters for typical atmospheric conditions, except in regions where surface temperatures are over 300 K and the temperature contrast between the surface and the air is larger than 10 K (Worden et al., 2007). However, retrievals of the lower free troposphere may show evidence of pollutants recently lofted from the boundary layer. In the context of the vertically smooth averaging kernels of the TES measurements we consider the lower free troposphere to range from approximately 850–550 hPa. For that purpose we chose to examine the $O_3$ and corresponding CO distributions at the 681 hPa retrieval level for which TES should have good sensitivity. We also examined the distributions at the 316 hPa level to contrast the upper and lower tropospheric distributions and to gain insight into different mechanisms controlling the lower free tropospheric $O_3$ in the export region of North America.

The TES retrieval products contain diagnostic information and flags for screening out failed profiles or those with reduced sensitivity (Osterman et al., 2006b; Kulawik et al., 2006). We used the general retrieval quality flag which removes the most suspect profiles. In addition, we screened

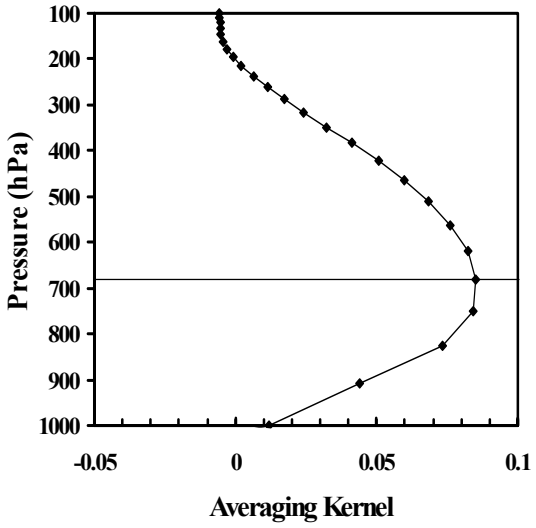


**Fig. 1.** TES averaging kernel for 681 hPa $O_3$ for profile near 31° N and 74° W on 6 April 2006. A horizontal line marks the 681 hPa level.

for clouds since they can impact the retrievals. For instance, Kulawik et al. (2006) estimated that the TES sensitivity to $O_3$ below a cloud with an optical depth of 1.0 will drop to approximately 30% of the clear sky sensitivity. The TES retrievals included information on cloud optical depth and cloud top pressure. The choice of a cloud optical depth threshold is complicated by the fact that the sensitivity below the cloud is influenced not only by the cloud optical depth, but also the temperature, surface conditions, and $O_3$ concentration. However, simulations of $O_3$ retrievals seemed to indicate that errors in retrieved total column and tropospheric column in the presence of low clouds increased at optical depths of 0.75 and above (see Fig. 7, Kulawik et al., 2006). Therefore we screened out any retrieval with an average cloud optical depth in the 1000–1250 $cm^{-1}$ $O_3$ retrieval band greater than this value. For consistency we used the same optical depth threshold for the CO retrievals but also included the average cloud optical depth in the 2000–2200 $cm^{-1}$ CO band. We used cloud top pressure in combination with the cloud optical depth thresholds so that we would not screen out retrievals that were above the clouds with an additional small margin of error added to the reported cloud top. That is we only applied the cloud screening for 681 hPa retrievals with cloud top pressure <700 hPa and for 316 hPa retrievals with cloud top pressure <350 hPa. Finally, we screened the remaining data for overall measurement sensitivity at a particular retrieval level using the averaging kernel matrix, which is provided as a post-processing diagnostic. Retrievals were eliminated if the diagonal values at the analysis level (681 or 316 hPa) were less than 0.01.

TES retrievals use the optimal estimation approach described by Rodgers (2000). The retrievals require an a priori

constraint to ensure mathematical uniqueness. For $O_3$ and CO the constraint consists of a priori profiles and covariance matrices from a climatology developed using the MOZART model (Brasseur et al., 1998). The climatological a priori is made up of MOZART profiles averaged monthly over $10^\circ \times 60^\circ$ latitude-longitude boxes (Bowman et al., 2006). The geographically variable a priori adds artificial structure, which can potentially obscure some of the real geographical variability of a trace gas. This artifact can be removed by reprocessing the TES $O_3$ and CO profiles with a universal a priori using a procedure developed by Zhang et al. (2006). We generated a universal a priori by averaging all original a prior profiles in the 60° N–60° S band and reprocessed the TES $O_3$ and CO data following Zhang et al. (2006). Hereafter in this study all of the TES data presented will refer to the reprocessed data.

### 2.2 Meteorological analyses

We used Global Final Analysis (FNL) data from the National Centers for Environmental Prediction (NCEP) to identify the predominant atmospheric circulation patterns over eastern North America and the North Atlantic Ocean during the time period 2000–2006. FNL products are available for 4 time intervals each day (00:00, 06:00, 12:00, and 18:00 UTC) on a $1^\circ \times 1^\circ$ horizontal grid at the surface and 26 pressure levels between 1000 and 10 hPa (http://dss.ucar.edu/datasets/ds083.2).

In addition, we used HYSPLIT (Draxler and Rolph, 2003, http://www.arl.noaa.gov/ready/hysplit4.html) backward trajectories to aid us in determining the likely source regions for any $O_3$ and CO enhancements observed in the TES data downstream of North America. The HYSPLIT model was used in single trajectory and ensemble mode with both Global Data Assimilation System (GDAS) (Derber et al., 1991; http://www.arl.noaa.gov/ss/transport/gdas1.html) and Eta Data Assimilation System (EDAS) (http://www.arl.noaa.gov/ss/transport/edas40.html) inputs. The GDAS data were on a $1^\circ \times 1^\circ$ global grid and with vertical coverage from the surface to 20 hPa. The EDAS data were on a horizontal grid with 40 km spacing centered over the continental US and extending northward into Canada to approximately 60° N, southward into Mexico to approximately 15° N, westward into the Pacific Ocean to approximately 140° W and eastward into the Atlantic Ocean to approximately 60° W (http://www.arl.noaa.gov/data/archives/edas40/EDAS40.gif). The EDAS data extended vertically from the surface to 50 hPa. In the ensemble mode HYSPLIT generates a set of 27 trajectories by shifting the meteorological input fields by one grid point each in the east, west and vertical directions. By doing so the ensemble gives the probable range of possible trajectories from a given location. This is helpful for circulation patterns with a high degree of spatial variability in which a small error in the selection of the starting point or in the meteorological input fields can result in large differences in trajectory pathways.

We also investigated the link between observed tropospheric $O_3$ enhancements and stratospheric intrusions using isentropic potential vorticity from the NCAR/NCEP $2.5^\circ \times 2.5^\circ$ Reanalysis (NNRA, http://www.cdc.noaa.gov/cdc/reanalysis). The NNRA isentropic potential vorticity analyses were available 4 times per day (00:00, 06:00, 12:00, and 18:00 UTC) at 11 isentropic levels for 270, 280, 290, 300, 315, 330, 350, 400, 450, 550, and $-650$ K. We interpolated these data to constant pressure levels to facilitate use with NCEP FNL analyses and TES retrievals which were also on pressure levels.

### 2.3 Circulation classification

Synoptic-scale circulation patterns over the North Atlantic were classified by applying the correlation-based map typing algorithm of Lund (1963) to the NCEP FNL sea level pressure (SLP) fields. This technique has been successfully applied to synoptic classification of summertime circulation patterns over the northeastern United States using the NCEP grids (Hegarty et al., 2007). In brief, the algorithm calculates a correlation coefficient between the grids representing scalar meteorological analysis fields over a given spatial domain at different times. The map types are selected using a critical correlation coefficient (i.e., 0.6), and then all the days in a given study period are classified as one of these types based on the degree of correlation.

Typically either the SLP or upper-level geopotential height (GPH) fields are chosen to represent the circulation patterns in the map typing algorithm. We found that, in comparison to SLP, the classification of the upper-level GPH was much less accurate with many patterns being incorrectly classified based on our subjective judgment of a representative sample. This is because the upper-level GPH fields tended to have smoother and less distinct features than SLP. Therefore we settled on using the SLP fields which are usually correlated with the upper–level patterns and yet exhibit distinct synoptic features such as cyclones, anticyclones and frontal troughs.

The map typing domain extended from 35° N to 50° N latitude and from 80° W to 50° W longitude (Fig. 2a). It covered much of the northeastern coast of the United States including the Washington D.C. to Boston megalopolis and extended eastward about a third of the way across the North Atlantic Ocean. The dimensions of the map typing domain were chosen to be just large enough to identify the unique synoptic features of each circulation pattern along the midlatitudes of the North American east coast, which we hypothesized to be important controls on pollutant export, but small enough to ensure accuracy in the synoptic classification. Synoptic patterns over larger domains are more difficult to classify because of the additional spatial variability inherently present over a greater area. To examine the larger-scale

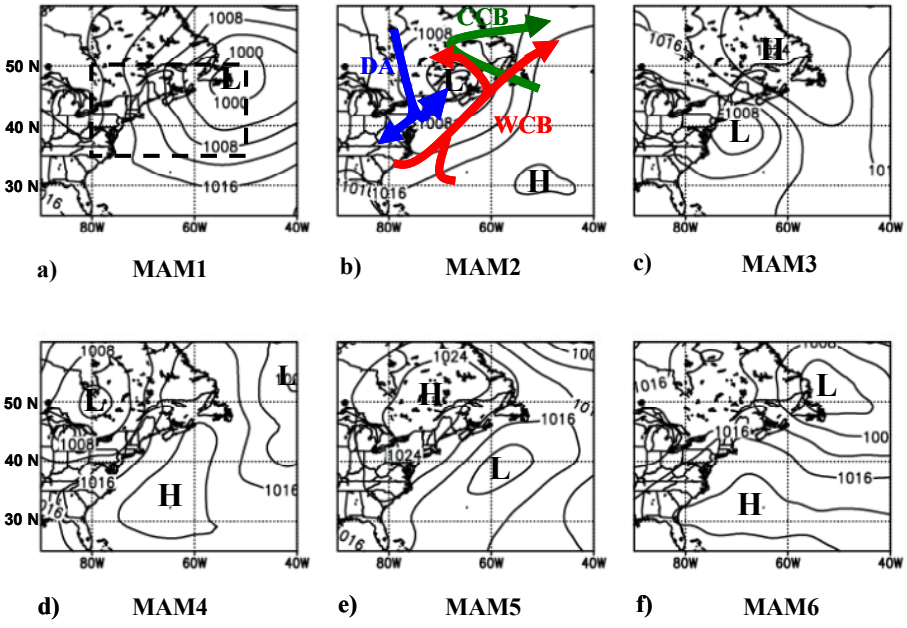


**Fig. 2.** Composite sea level pressure (hPa) analyses from 2005–2006 for map types MAM1-MAM6 **(a–f)**. The boundaries of the map typing domain are shown as dashed lines on a) and schematic representations of the warm conveyor belt (red curve), dry airstream (blue curve) and cold conveyor belt (green curve) are shown on b).

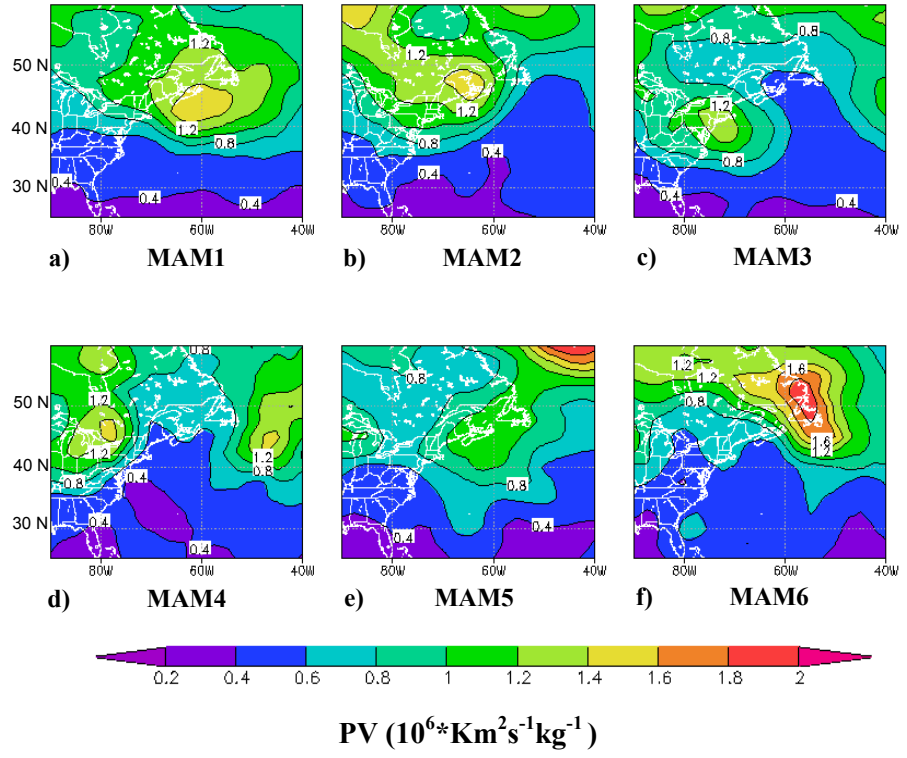


**Fig. 3.** Mean 400 hPa potential vorticity (PV) for MAM1-MAM6 interpolated from the isentropic surfaces of the NCAR/NCEP Reanalysis **(a–f)**. 1 PVU is $10^6$*Km$^2$s$^{-1}$kg$^{-1}$.

**Table 1.** Map types and meteorological characteristics.

| Map Type | 2005–2006 Frequency (%) | Characteristics |
|---|---|---|
| MAM1 | 24 | – Large semi-stationary low pressure center east of Newfoundland<br>– Persistent subsiding northwest flow over northeast US<br>– Rising motion due to weak cyclonic disturbances to the south and WCB well offshore |
| MAM2 | 19 | – Cyclone tracking into northern New England and Canadian Maritimes<br>– Some weak secondary coastal development,<br>– Rising motion along east coast and offshore in WCB |
| MAM3 | 15 | – Developing coastal cyclone possibly associated with mature cyclone inland,<br>– East-northeast flow along coast with<br>– Rising motion over the ocean and northern coastal areas in WCB<br>– Some cyclones persistent particularly in late spring |
| MAM4 | 5 | – Anticyclone offshore<br>– Subsiding flow over ocean near coast<br>– Strong descent in DA of cyclone well out to sea |
| MAM5 | 11 | – Cyclone offshore with WCB rising motion to the south and east and DA descent between cyclone and coast<br>– Anticyclone in southeastern Canada with weak subsidence right along east coast |
| MAM6 | 7 | – Large subtropical anticyclone off east coast<br>– Weak subsidence along US coast and immediately offshore in light southwesterly and westerly<br>– Cyclone center near Labrador with DA descent in northwest flow over Canadian Atlantic provinces extending out to sea |

impact of the circulation patterns on the tropospheric distributions of $O_3$ and CO exported from North America the map typing domain was embedded into a larger study domain which extended from 25° N to 60° N and from 90° W to 40° W (Fig. 2a).

## 3 Synoptic circulation classification

We classified days based on six map types (denoted as MAM1-MAM6) identified for the spring seasons of 2005–2006 when TES V002 data were available. The map type frequencies and the important meteorological features associated with each map type are summarized in Table 1. These six map types were representative of the circulation patterns on approximately 81% of the days in 2005 and 2006. Of course there were other patterns that might be relevant to export from North America, but they occurred too infrequently to enable a meaningful interpretation of their average export patterns and therefore they are not considered in this study. Here we present a brief discussion as to how the six predominant patterns might relate to the major hypothesized transport pathways. In Sect. 4 we discuss in detail the impact of these circulation patterns on the tropospheric $O_3$ distributions observed by TES.

Map type MAM1 was the most frequent pattern, occurring on 24% of the days in springs 2005–2006 (Table 1). It featured a large, intense, and closed low centered east of Newfoundland, Canada (Fig. 2a), which was typically the result of a rapidly deepening cyclone migrating northeastward along the US east coast. Often these systems become so large and vertically deep that they disrupt the normal west to east progression of storm systems and they become quasi-stationary. Analysis of the sequencing of map types indicated that MAM1 typically persisted for 2–4 days in a row with a maximum duration of up to 10 days, particularly early in the season. The persistent pattern could thus produce a well-stirred region of the atmosphere that continuously interleaves air masses originating from many areas of the lower, mid- and upper troposphere as well as the lower stratosphere with the vertical layering allowing for mixing to occur at the boundaries of the air masses. Another characteristic of MAM1 was that the surface low was typically associated with a closed upper-level circulation that extended above the 300 hPa pressure level and with 400 hPa potential vorticity (PV) $>1.4$ potential vorticity units (PVU) on its western side (Fig. 3a). The tropopause is typically defined as falling between 1 (Shapiro, 1987) and 2 PVU (Appenzeller et al., 1996; Lamarque et al., 1996; Parrish et al., 2000). Therefore PV values over the range of 1–2 PVU extending down into the troposphere are typically regions of stratospheric intrusions. This indicates that in MAM1 stratospheric influence reached at least as low as the 400 hPa level in a region centered between the Canadian Maritimes and Newfoundland,

which may explain the higher levels of the 681 hPa $O_3$ there as discussed in Sect. 4.1.

Map types MAM2 and MAM3 depict smaller and generally more mobile cyclones near the east coast (Fig. 2b–c). These systems occurred on a total of 50% of the spring days in 2005–2006 and typically featured distinct ascending and descending air streams (Table 1). The WCB, one of the main ascending streams, is located to the east of the cold front and generally originates in the lower troposphere (Carlson, 1980; Eckhardt et al., 2004). In the Northern Hemisphere the WCB is located on the eastern side of an upper level trough and ascends into the mid- and upper troposphere on a general southwest to northeast trajectory (Fig. 2b). The WCB may be intercepted by the fast moving upper level winds that transport pollutants rapidly downstream of the cyclone. This process has been documented through aircraft measurements (Cooper et al., 2001, 2002; Parrish et al., 2000; Stohl and Trickl, 1999; Stohl et al., 2003b; Trickl et al, 2003). This transport pathway is also described by Owen et al. (2006) with regards to transport to the Azores.

Note that a part of the WCB, termed the secondary WCB, may branch off to the west and turn cyclonically around the center of the low. Steered by the northwesterly winds on the western side of the low the air mass can experience isentropic descent into the mid and lower troposphere (Fig. 2b). This pathway could also be an important mechanism for transporting pollutants from the urban areas of the US east coast to the lower free troposphere of the western North Atlantic. The other major ascending air stream is the cold conveyor belt (CCB) (Fig. 2b) (Carlson, 1980). For east coast cyclones this airstream typically originates from the lower troposphere over the ocean where it intercepts primarily aged air, but it can entrain pollution as it heads west across eastern North America. However, it occurs characteristically within very cloudy regions not conducive to photochemical production of $O_3$ (Cooper et al., 2001, 2002).

The main descending airstream of the cyclone is usually referred to as the dry airstream (DA) (Fig. 2b) because it transports drier air from the upper troposphere and lower stratosphere to the mid-troposphere with some strong systems allowing for direct transport to the lower troposphere (Carlson, 1980; Cooper et al., 2002). Along with low humidity the air transported in the DA is also normally $O_3$-rich and therefore influences the $O_3$ distributions of the lower troposphere (Cooper et al., 2001, 2002; Merrill et al., 1996; Moody et al., 1996; Oltmans et al., 1996; Cooper et al., 2001, 2002).

The differences in the map types MAM2 and MAM3 were mainly due to the position and history of the cyclones. The cyclones depicted in MAM2 were generally mature systems that had tracked from the central US to the Canadian Maritimes over several days. The WCB of these systems possibly encountered many high emission regions of eastern North America. The MAM3 map type depicted cyclones that developed along the US east coast with areas of easterly flow in northeastern states. In late spring the MAM3 pattern tended toward episodes of persistence as small cyclones developed along the coast to the east of an inland upper-level cut-off low, and then stalled along the coast or rotated back around the inland system. For example in both May 2005 and 2006 there were episodes of MAM3 which persisted for 6 days or more.

Map types MAM4-MAM6 featured anticyclones along the US east coast with cyclones well inland or out to sea, and thus for these map types WCB lofting of continental boundary layer air was less influential than for map types MAM2 and MAM3. However, the DAs to the rear of the ocean cyclones of MAM4 and MAM5 seemed to influence areas of the western North Atlantic Ocean as will be discussed in Sect. 4. Map type MAM6 occurring on only 7% of the days, featured a broader subtropical anticyclone centered off the east coast extending well out to sea and westward into the southeastern US with a cyclone well to the northeast near Labrador. Such a circulation pattern typically produces a large area of weak subsidence extending from the east coast to the central North Atlantic Ocean restricting synoptic-scale lofting of boundary layer pollutants to the free troposphere. Furthermore, the northerly location of the cyclone and its orientation shown in Fig. 2f suggests that the influence of the DA might also be weak throughout most of our study domain; leading to generally smooth pollutant distributions.

## 4 Association between $O_3$ distributions and circulation types

Composites of the 681 hPa and 316 hPa $O_3$ and CO for the entire season and individual map types were created by interpolating measurements from the orbital overpasses to a $1^\circ \times 1^\circ$ grid using a Gaussian weighting scheme similar to that described in Luo et al. (2002). If no observations existed within 350 km of a grid point, typically because of quality or cloud screening, this point was masked out of the analysis.

First, we created full seasonal composites for the 681 hPa $O_3$ and CO which included all the observations regardless of map type (Fig. 4). The mean 681 hPa $O_3$ seasonal composite indicated elevated levels (55–65 ppbv) over the western Atlantic Ocean south of 45° N, ∼1000 km downwind of the US (Fig. 4a). There was a corresponding feature in the mean CO composite with mixing ratios of 115–125 ppbv forming a belt emanating from the US east coast that dissipated and narrowed before turning northeastward following the prevailing lower tropospheric wind flow (Fig. 4b). In the area of highest CO extending from the US coast, between 75° W – 55° W and 30° N – 45° N (denoted hereafter as Region 1), we found a slight positive correlation of 0.22 between $O_3$ and CO with a slope of 0.13 mol mol$^{-1}$ statistically significant at the $p$=0.01 level (Fig. 5a and Table 2). However, further to the north and east in a region bounded by 45° N – 55° N and 65° W – 45° W (referred to hereafter as Region 2), where $O_3$

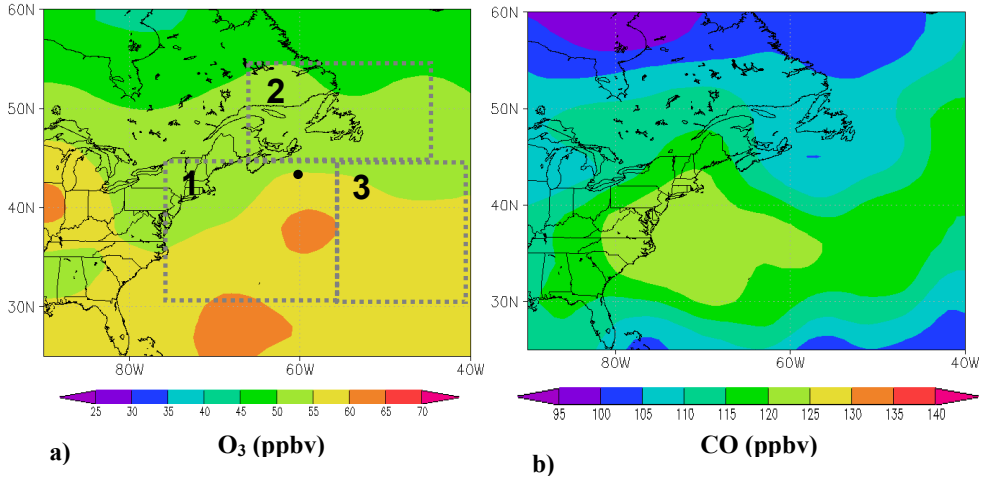


**Fig. 4.** Spring seasonal composites for 2005-2006 of **(a)** TES 681 hPa $O_3$ (ppbv) and **(b)** TES 681 hPa CO (ppbv). In (a) the borders of Regions 1, 2, and 3 are shown as dashed lines and the location of Sable Island, NS is shown as a black dot.

**Table 2.** $O_3$-CO slopes, correlation coefficient ($r$) and sample size ($N$) for selected circulation types in the three regions shown in Fig. 4a.

| | Region 1 | Region 2 | Region 3 |
|---|---|---|---|
| All | 0.13[a] (0.22) $N$=226 | −0.11 (−0.16) $N$=93 | 0.17[a] (0.29) $N$=184 |
| MAM1 | 0.12[c] (0.26) $N$=58 | −0.24 (−0.32) $N$=22 | 0.20[a] (0.34) $N$=65 |
| MAM2 | 0.19[c] (0.27) $N$=41 | −0.11 (−0.30) $N$=19 | 0.27[b] (0.34) $N$=34 |
| MAM3 | 0.20[c] (0.32) $N$=31 | 0.38[b] (0.62) $N$=13 | 0.29[c] (0.40) $N$=23 |

gradually dropped off to 50–55 ppbv, there was virtually no $O_3$-CO correlation (Fig. 5b, Table 2).

The correlation of observed $O_3$ and CO is a useful diagnostic indicator of the photochemical processing of an air mass, and the $O_3$-CO slope value can be used to estimate the influence of exported anthropogenic pollutants and the efficiency of photochemical $O_3$ production (Parrish et al., 1993, 1998; Mao et al., 2004). A large number of measurements at surface sites in eastern North America have indicated that typical summertime $O_3$-CO slopes range from 0.2–0.35 mol mol$^{-1}$ (Parrish et al., 1993, 1998; Chin et al., 1994; Mao et al., 2004). Aircraft measurements during the NARE93 and ICARTT 2004 summer campaigns indicated similar slopes, which took place in the lower free troposphere just east of the North American coastline (Daum et al., 1996; Zhang et al., 2006). Fewer studies have been conducted for springtime, but analysis of spring measurements over 4 years in the 1990s at Sable Island, Nova Scotia indicated that the $O_3$-CO slope increases dramatically from near zero in March to approximately 0.35 mol mol$^{-1}$ in May (Parrish et al., 1998).

We acknowledge that care must be taken in comparing the $O_3$-CO slopes to earlier studies due to changing emissions of $NO_x$ and CO in North America over time which may have impacted typical $O_3$-CO slopes (Parrish et al., 2006; Kim et al., 2006). Nonetheless, our free tropospheric value of 0.13 mol mol$^{-1}$ in Region 1 falls in the middle of this range and suggests that similar to summertime the pollutant plumes lofted to the free troposphere retain their near surface features. In Region 2, the lack of $O_3$-CO correlation indicated no significant photochemical production due to either limited sunshine or the lack of fresh exported pollutants. The fact that this area showed a relative minimum in CO (Fig. 4b) suggests that the lack of exported pollutants was a more critical factor.

The seasonal composites of Fig. 4 and the seasonal $O_3$-CO slopes showed strong evidence of continental export to the lower free troposphere. However, it should be noted that the cloud screening removed approximately 36% of the 681 hPa retrievals from the composite analyses and therefore the distributions are more representative of clear-sky or thin cloud cover conditions. Crawford et al. (2003) made the case using data from the TRACE-P aircraft campaign that pollutant levels should have a positive bias in cloudy areas. Therefore, the actual export signal could be even greater than that depicted in the TES composites. The export signal captured by TES comes mainly from portions of cyclonic airstreams conducive to export but with thin or broken cloud cover as is discussed in Sect. 5.

All the TES retrievals for the months of March – May 2005 and 2006 were also grouped based on the map type classification for the calendar day of the orbital overpass.

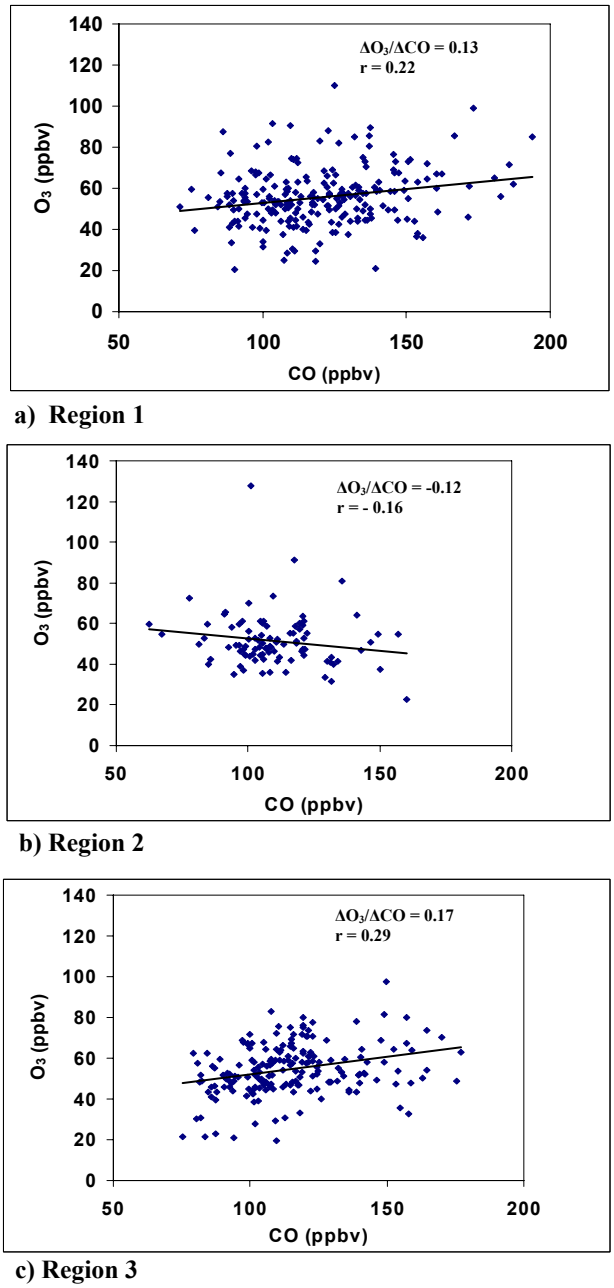


**Fig. 5.** Scatter plots of TES 681 hPa $O_3$ versus CO retrievals during MAM 2005–2006 for **(a)** Region 1, **(b)** Region 2 and **(c)** Region 3.

The resulting composite distributions for 681 hPa $O_3$ and CO for each of the six map types are shown in Fig. 6. Composites of HYSPLIT 4-day back trajectories for each map type in Region 1 and for MAM1 in Region 2 were created to help illustrate some of the transport patterns into these regions and are shown in Figs. 7 and 8, respectively. The trajectory composites were created by launching a single back trajectory using GDAS meteorological data from each of the TES locations in the respective regions from an altitude of 3500 m a.m.s.l.

**Table 3.** The percentage of 4-day back trajectories starting from TES observation locations in Region 1 at 681 hPa that pass below listed pressure levels over North America between 15–65° N and 125–70° W for map types MAM1-MAM6 and for a random set of locations and times (1 per day during MAM 2006) denoted as RAN.

| | (%) Below 700 hPa | (%) Below 800 hPa | % Below 900 hPa | *N* |
|---|---|---|---|---|
| MAM1 | 30 | 12 | 6 | 117 |
| MAM2 | 44 | 17 | 6 | 98 |
| MAM3 | 52 | 33 | 13 | 61 |
| MAM4 | 4 | 0 | 0 | 23 |
| MAM5 | 26 | 12 | 9 | 43 |
| MAM6 | 25 | 13 | 5 | 40 |
| RAN | 43 | 26 | 11 | 92 |

which approximately corresponded to the 681 hPa pressure level. Additionally composite distributions for 316 hPa $O_3$ and CO for each map type are shown in Fig. 9. The $O_3$ and CO distributions corresponding to each of the six map types are discussed in Sects. 4.1–4.3 which follow.

### 4.1 MAM1

The 681 hPa $O_3$ levels for MAM1 were slightly elevated (∼55–60 ppbv) in a region extending from the Canadian Maritimes and Newfoundland southward over the western North Atlantic Ocean (Fig. 6a). The circulation pattern, featuring the intense persistent low near Newfoundland, produced distinct chemical characteristics in Regions 1 and 2 reflected in the $O_3$-CO relationship (Fig. 6a, g, Table 2).

Region 1 had a large offshore area of 681 hPa composite $O_3$ mixing ratios ranging from 55 to 60 ppbv corresponding to a belt of slightly elevated CO (120–125 ppbv) (Fig. 6a and g). The presence of both elevated $O_3$ and CO levels in Region 1 produced a positive $O_3$-CO slope of 0.12 mol mol$^{-1}$ which was statistically significant at the $p$=0.10 level (Table 2) indicating some anthropogenic influence. The composite of back trajectories indicated that the majority of the air arriving in this region descended from the mid- and upper troposphere on northwesterly flow, as would be expected given the pressure pattern of MAM1 (Figs. 2a and 7a). However, a few trajectories ascending from the Gulf Coast area could have injected anthropogenic pollutants into the large circulation systems which may explain the positive $O_3$-CO correlation. These ascending trajectories, 30% of which passed below 700 hPa over North America (Table 3), were associated with the mobile cyclones preceding the development of the large semi-stationary cyclone or other smaller ones that may have traveled southeastward along the

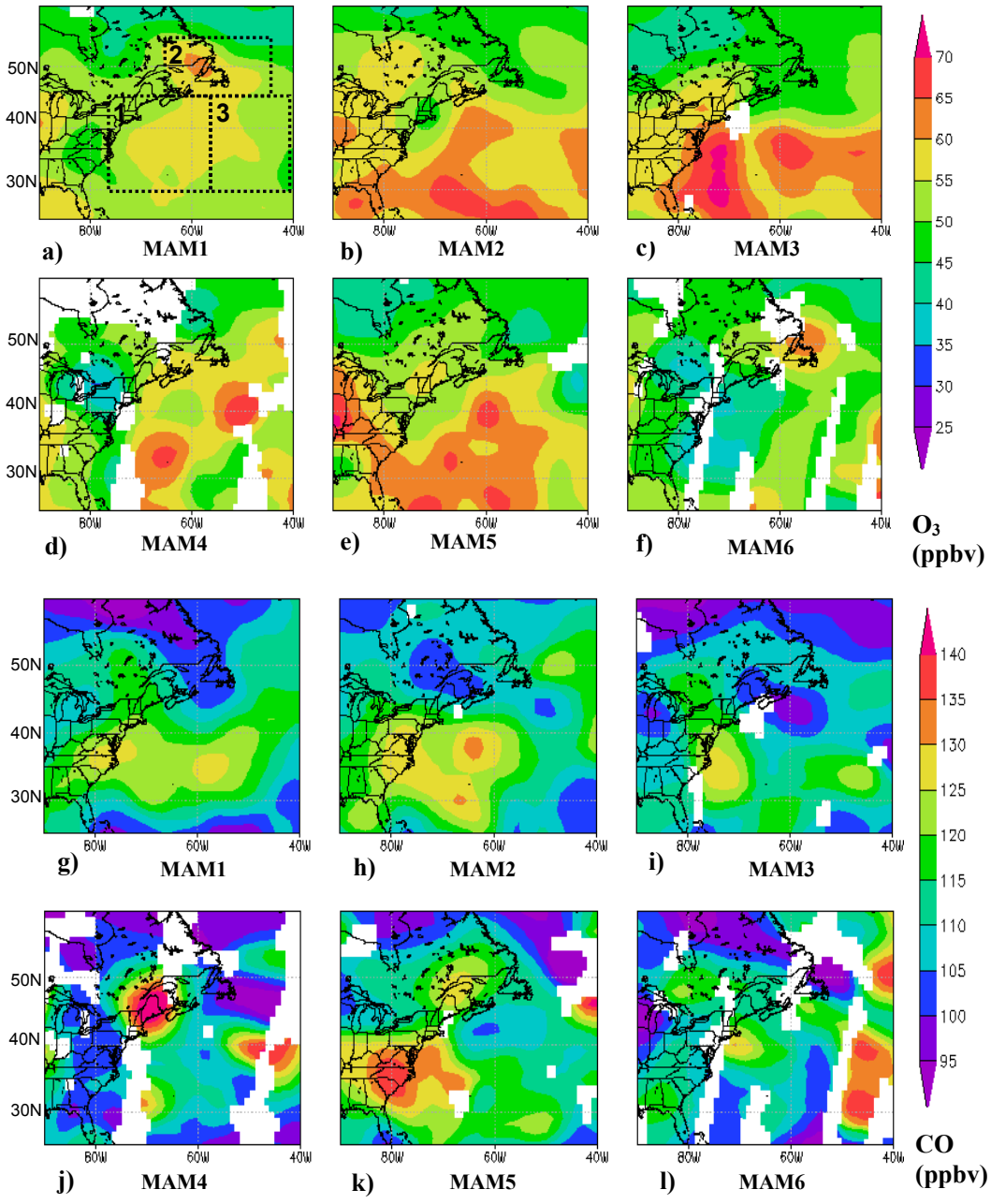


**Fig. 6.** 681 hPa composites for MAM1-MAM6 for $O_3$ (ppbv) **(a–f)** and CO (ppbv) **(g–l)**. In a) the borders of Regions 1, 2, and 3 are shown as dashed lines.

southwest corner of the main circulation. In addition approximately 20% of the 4-day back trajectories had circulated around from the eastern side of the low center, predominantly from altitudes below 600 hPa, following a long ascending path through northeastern Canada before arriving back in Region 1 on descending northwesterly flow. This long path suggests that any pollutants entrained into these types of closed circulation patterns from this region could potentially circulate around the large system over several days with gradual dilution and chemical transformation, which would contribute to the relatively uniform moderate enhancements in $O_3$ and CO levels.

Region 2 featured $O_3$ mixing ratios 60–65 ppbv and relatively low CO (100–105 ppbv in the center of the region (Fig. 6g), which yielded a negative $O_3$-CO correlation of $r=-0.16$ (Fig. 5b, Table 2). This region was also associated

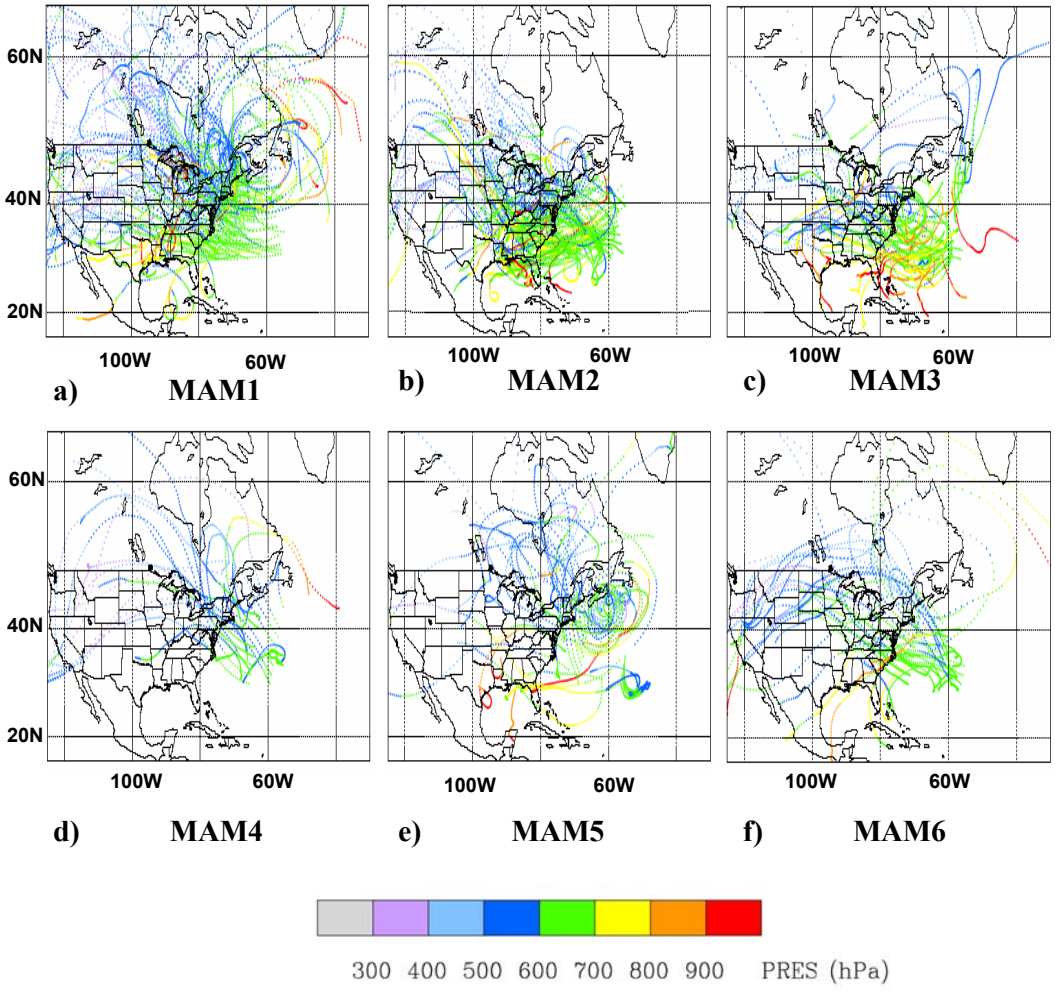


**Fig. 7.** Four-day HYSPLIT back trajectories using GDAS data from locations of TES 681 hPa observations in Region 1 for map types MAM1-MAM6 **(a–f)**. The colors indicate the pressure levels (hPa) of the trajectory parcels.

with an extensive area of elevated $O_3$ (>160 ppbv) at the 316 hPa level (Fig. 9a) and elevated PV values (>1.5 PVU) at the 400 hPa level (Fig. 3a). These factors, combined with a lack of ascending trajectories over continental sources of pollutants (Fig. 8), suggested that the enhanced tropospheric $O_3$ mixing ratios in Region 2 over the Canadian Maritimes and Newfoundland were likely a result of stratospheric inputs associated with the deep low pressure system. It should be cautioned that this enhancement in 681 hPa $O_3$ could also be partly a result of a shift toward higher altitudes (400–500 hPa) of the peak 681 hPa $O_3$ averaging kernels (not shown) in retrieval calculations. The shape of the averaging kernels can be impacted by non-related meteorological parameters such as temperature, water vapor, and clouds, and by the vertical distribution of $O_3$ itself. Therefore, this shift could just be a reflection of the greater concentrations at higher altitudes and may not extend all the way down to 681 hPa.

### 4.2 MAM2 and MAM3

The smaller and more dynamic cyclonic systems located near the US coast in MAM2 and MAM3 produced $O_3$ and CO composite distributions with greater spatial contrast compared to those in MAM1. At 681 hPa there was a general area of enhanced $O_3$ mixing ratios (>60 ppbv) extending from just off the US coast to ~50° W south of ~45° N (Fig. 6b and c). Enhanced $O_3$ roughly corresponded to enhanced CO (>120 ppbv), particularly near the US coast (Fig. 6h and i). The location of the enhanced $O_3$ and CO near and to the east of storm centers and downwind of the US coast suggests that lofting of the pollutants from the continental boundary layer by the WCB airstreams played a major role in producing the enhanced $O_3$ levels for these map types.

The 4-day back trajectory composites for MAM2 and MAM3 showed that the majority of trajectories arriving in Region 1 came from the south and west which is consistent with WCB flow (Fig. 7b and c). Some of the trajectories

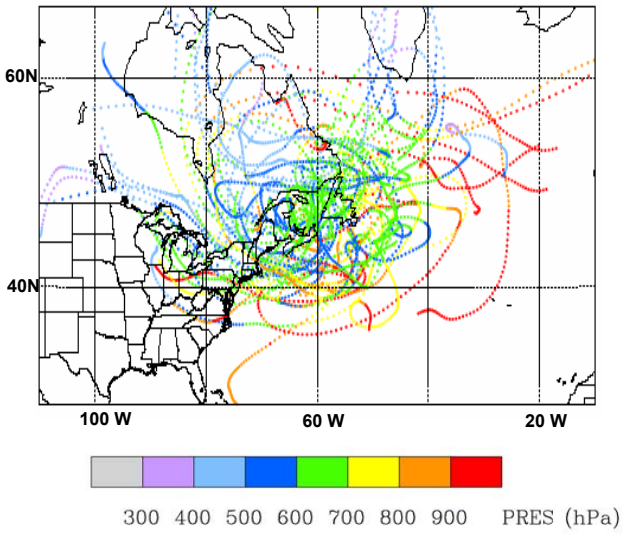


**Fig. 8.** Four-day HYSPLIT back trajectories using GDAS data from locations of TES 681 hPa observations in Region 2 for map type MAM1. The colors indicate the pressure levels (hPa) of the trajectory parcels.

showed a circulation around the back of the low center in the secondary WCB branch passing over urban areas of the northeastern US. Furthermore, 44–52% of the trajectories passed below the 700 hPa level and 17–33% passed below the 800 hPa level over the continent before finally being lofted to the 681 hPa level (Table 3). These percentages are notably greater than for any other map types and help explain the greater $O_3$ and CO levels in this region due to a stronger influence of WCB lofting. The fact that the percentages of lofting trajectories for MAM2 and MAM3 are only slightly greater than for a random sampling of locations, shown in the last row of Table 3, may be partly explained by the fact that the locations of the good TES retrievals are biased towards areas with less cloud cover. We caution that trajectories based on $1^\circ \times 1^\circ$ meteorological data may not accurately resolve the transport from the continental boundary layer and these percentages should be used to gauge the relative likelihood of receiving boundary layer air.

There were some differences in the 681 hPa $O_3$ and CO distributions between MAM2 and MAM3. For example the area of high $O_3$ over the ocean for MAM2 was generally off of the US coast at latitudes north of the Carolina states, whereas for MAM3 it extended all the way to the coast and even inland. In addition, the CO enhancement in MAM3 was less and dropped off to the east more quickly than in MAM2. These differences are due in part to the circulation patterns. The MAM2 circulation featured a low over land with basically westerly to southwesterly flow at the coast, while the high and low pair in MAM3 resulted in an easterly component to the flow along the northern parts of the coast. Thus, for MAM2 the pollutants would be transported away from the coast, while for MAM3 some of the continental outflow might be re-circulated back toward the coast.

In general, we found that the 681 hPa $O_3$ and CO observations for map types MAM2, and MAM3 were positively correlated at $r$=0.27 and $r$=0.32, respectively, in Region 1 with corresponding positive slopes of 0.19 and 0.20 mol mol$^{-1}$ both significant at the $p$=0.10 level (Fig. 10, Table 2). These slopes are much lower than those reported by Zhang et al. (2006), who calculated a slope of 0.81 mol mol$^{-1}$ and a correlation of $r$=0.53 for lower tropospheric TES measurements near this region. However, this may be partially explained by the fact that their measurements were in July for a more compact region centered further south, while ours included a larger region centered further north and included the months of March and April when photochemical production is reduced.

Since WCB lofting to the upper troposphere is an important mechanism for continental export of pollution, we examined the TES 316 hPa composites for evidence of this transport mechanism. The CO composites showed areas of enhanced CO off the southeastern US coast particularly for MAM2 and MAM3. Correspondingly there were areas of enhanced CO in the lower troposphere (Fig. 6g and h). However, while most of the single GDAS 4-day back trajectories launched from each of the locations of the 316 hPa TES observations in this region showed general ascent from the south and west only 10% went below 700 hPa over the continent (not shown). In fact, even when the higher resolution EDAS data was used only one of the back trajectories for the 3 days in which 316 hPa CO was greatest (>115 ppbv) briefly encountered (<3 h) the lower troposphere (below 700 hPa) over the continent (not shown). In actuality pollutants were possibly lofted to the upper troposphere by convection, as suggested in previous studies (Kiley and Fuelberg et al., 2003; Li et al., 2006 and Kim et al., 2008), that was associated with the cold fronts of the passing cyclones. However, convection may not always be well resolved by the EDAS (40 km grid spacing) and GDAS ($1^\circ \times 1^\circ$ grid spacing) meteorological data input to the trajectory models.

The 316 hPa composite CO for MAM2 did suggest continental export in the region just southeast of Newfoundland with CO>150 ppbv. An ensemble of backward EDAS trajectories, launched from locations of TES 316 hPa observations for 2 of the 3 days coincident with the highest CO mixing ratios in this region suggested the sources were boundary layer air over the US Central Plains mixing with air that had traveled near the surface from the western Gulf of Mexico and near the Los Angeles Basin (not shown). Presumably air masses with fresh emissions from the east coast ascended slowly while moving rapidly in a general northeastward direction in the WCB and thus would not yet have reached this level within the confines of our study domain.

In addition to WCBs the DAs of the cyclones in MAM2 and MAM3 may have contributed to the $O_3$ enhancements

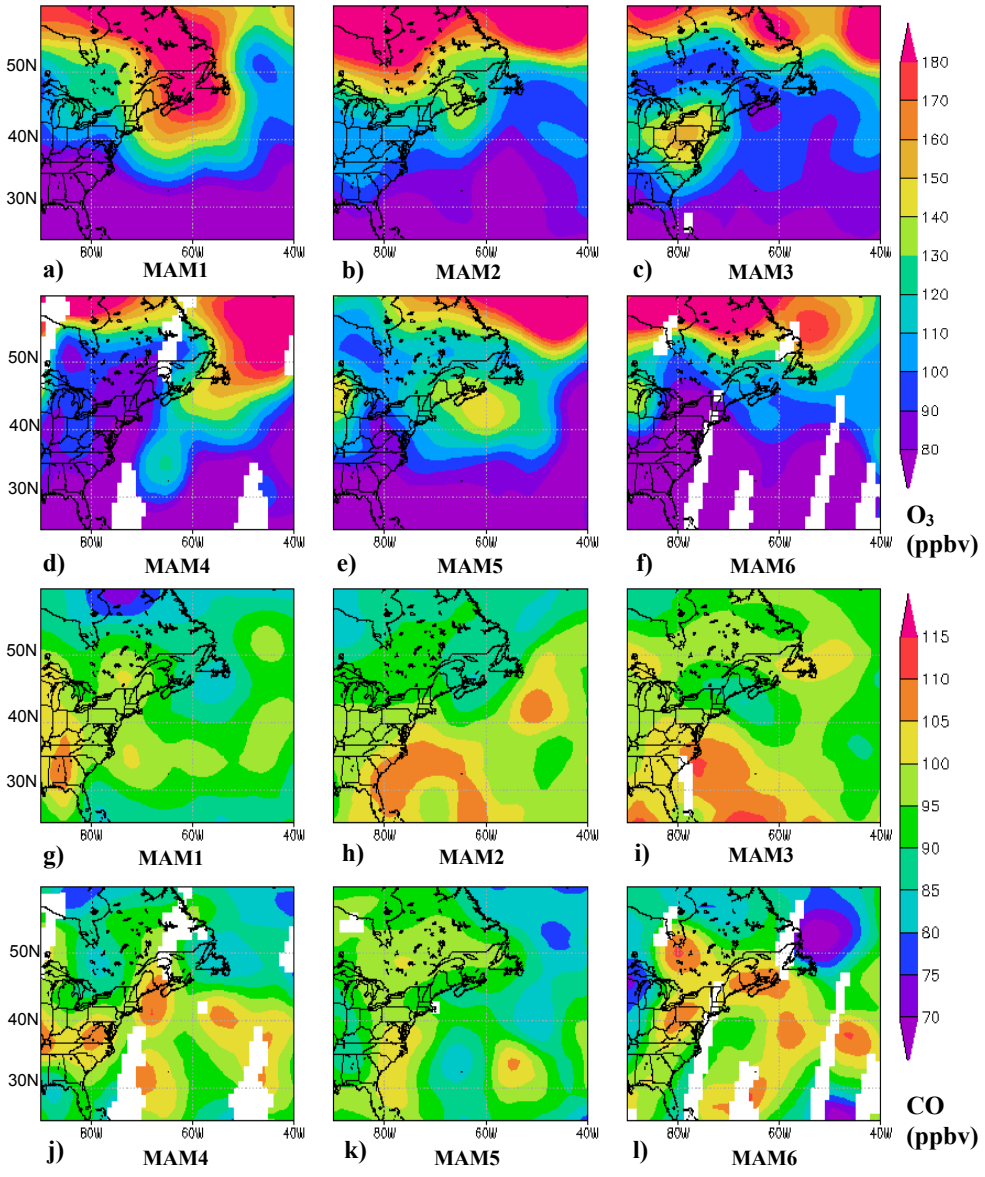


**Fig. 9.** 316 hPa composites for MAM1-MAM6 for $O_3$ (ppbv) **(a–f)** and CO (ppbv) **(g–l)**.

at 681 hPa, primarily in the northern areas of the study domain, by transporting stratospheric air down to lower tropospheric levels. For example, enhancements in 681 hPa $O_3$ over Nova Scotia in MAM2 and over the Mid-Atlantic states and New England for MAM3 corresponded to slightly enhanced 316 hPa $O_3$, 400 hPa PV >1 PVU, and descending back trajectories (Figs. 3b, c, 6b, c, 7b, c, and 9b, c). All these factors together imply stratospheric or upper tropospheric influences. However, in general, the 316 hPa and 681 hPa distributions of $O_3$ showed little spatial correlation, which reflected the different dominant processes at the two levels. That is, contributions from continental boundary layer pollution played a significant role in the lower troposphere over western North Atlantic Ocean, especially south of 45° N, while there was greater stratospheric influence in the upper troposphere at more northern latitudes.

### 4.3 MAM4, MAM5 and MAM6

The map types MAM4 – MAM6 featured predominantly anticyclonic flow along the east coast which generally seemed to reduce the continental export to the free troposphere over the western North Atlantic Ocean compared to MAM2 and MAM3. For both MAM4 and MAM5 there were enhanced 681 hPa $O_3$ levels (>55 ppbv) over the western North Atlantic Ocean extending from the coast of Florida

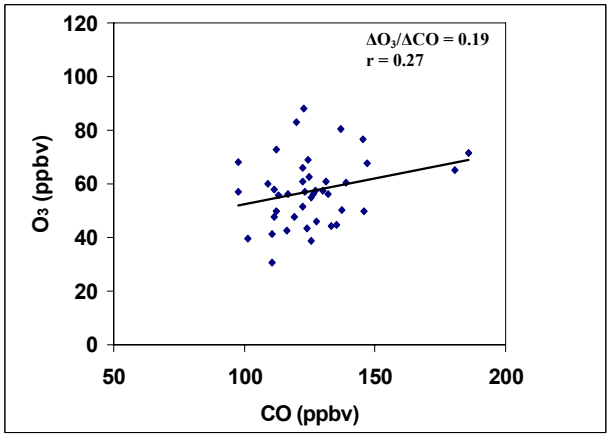


**a) MAM2**

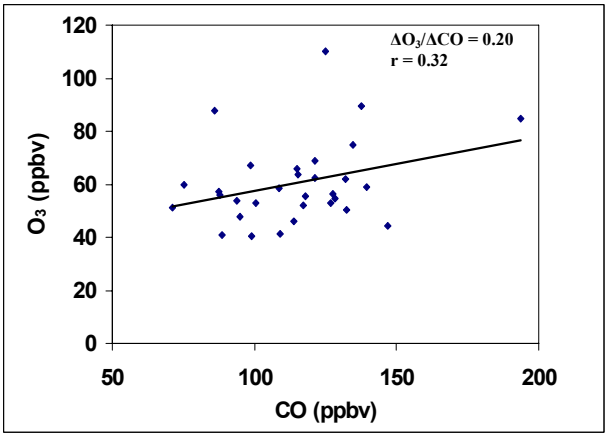


**b) MAM3**

**Fig. 10.** Scatter plots of TES 681 hPa $O_3$ versus CO retrievals in Region 1 for **(a)** MAM2 and **(b)** MAM3.

northeastward to east of Newfoundland and further out to sea (Fig. 6d and e). However, for these two map types the areas of enhanced 681 hPa CO did not always correspond to the areas of higher $O_3$ levels. Meanwhile for MAM6, both $O_3$ and CO at 681 hPa were generally low over most of the western North Atlantic Ocean. Overall, our interpretation of the composites for MAM4-MAM6 was made more difficult by the low frequency of occurrence of these map types. This together with the strict quality and cloud screening left too few points of coincident $O_3$ and CO observations available for calculating statistically significant slope and correlation values. We therefore did not include them in Table 2 and focused on the flow characteristics depicted in the SLP, PV and back trajectory composites.

For MAM4 some pollutants could have been circulated around the back of the cyclone further east in the Atlantic leading to enhanced $O_3$ and CO at 681 hPa near 60° N and 55° W (Fig. 6d and j). However the general area of high 681 hPa $O_3$ extending from east of Newfoundland southwestward to just east of Bermuda was associated with a wide range of CO levels from 105–140 ppbv (Fig. 6d and j). Therefore we looked for evidence of stratospheric or upper tropospheric influence and found that the 316 hPa $O_3$ composite showed a lobe of high $O_3$ extending southwestward from the central North Atlantic to west of Bermuda and composite back trajectories showed descending flow from higher latitudes southward to the lower troposphere over the mid-latitudes of the western North Atlantic Ocean (Fig. 7d). While the PV composite at 400 hPa did not indicate deep ozone intrusions (Fig. 3d) that might explain the enhanced $O_3$ at 681 hPa it is possible that short-lived stratospheric intrusions that were not evident in the seasonal PV average transported high $O_3$ air to the lower troposphere that remained there even after the intrusion dissipated. Unfortunately, further interpretation is limited by the sparse TES data coverage and the limited frequency (<7% of the days) of this map type.

For MAM5 the enhanced 681 hPa $O_3$ and CO off the coast of the southeastern US was possibly produced by WCB lofting of continental pollutants as the cyclones preceding the anticyclone tracked off the coast as suggested by a few trajectories of the composite analysis (Figs. 2e, 6e, k and 7e). The very enhanced CO inland over the southeastern US was coincidental and primarily reflected extreme measurements ranging from 144–191 ppbv on 20 April 2006, that were possibly a result of outflow from convective storms over Texas from the previous day being incorporated into the descending flow behind a somewhat larger and more intense MAM5 cyclone. There were other areas of enhanced $O_3$ over the ocean that corresponded to relatively low CO (<110 ppbv), e.g., the area near 40° N and 60° W. For this region, likely in the DA of the cyclone, enhanced $O_3$ at 316 hPa (Fig. 9e), PV>1 PVU at 400 hPa (Fig. 3e), and descending back trajectories initiated at the locations of the 681 hPa TES observations (Fig. 9e) all suggested stratospheric inputs as the cause. It should be noted that as with MAM1 there was a corresponding shift toward higher altitudes of the 681 hPa $O_3$ averaging kernels in this region. However, for MAM5 the averaging kernel peaks shifted upward to only 500–550 hPa and thus it seems more likely that for MAM5 the high levels of 681 hPa $O_3$ retrieved by TES in this region were actually due to high $O_3$ air making it all the way down to lower altitudes of the free troposphere.

The lowest 681 hPa $O_3$ levels in the western North Atlantic Ocean corresponded to circulation patterns of MAM6. For this map type composite $O_3$ levels in the western Atlantic were generally <55 ppbv with many areas, especially close to the US east coast, being <45 ppbv (Fig. 6f). The 681 hPa CO mixing ratios were also low in this region with composite values generally <110 ppbv with many areas <105 ppbv (Fig. 6l). We hypothesize that the large anticyclone centered near Bermuda and extending westward into the eastern US

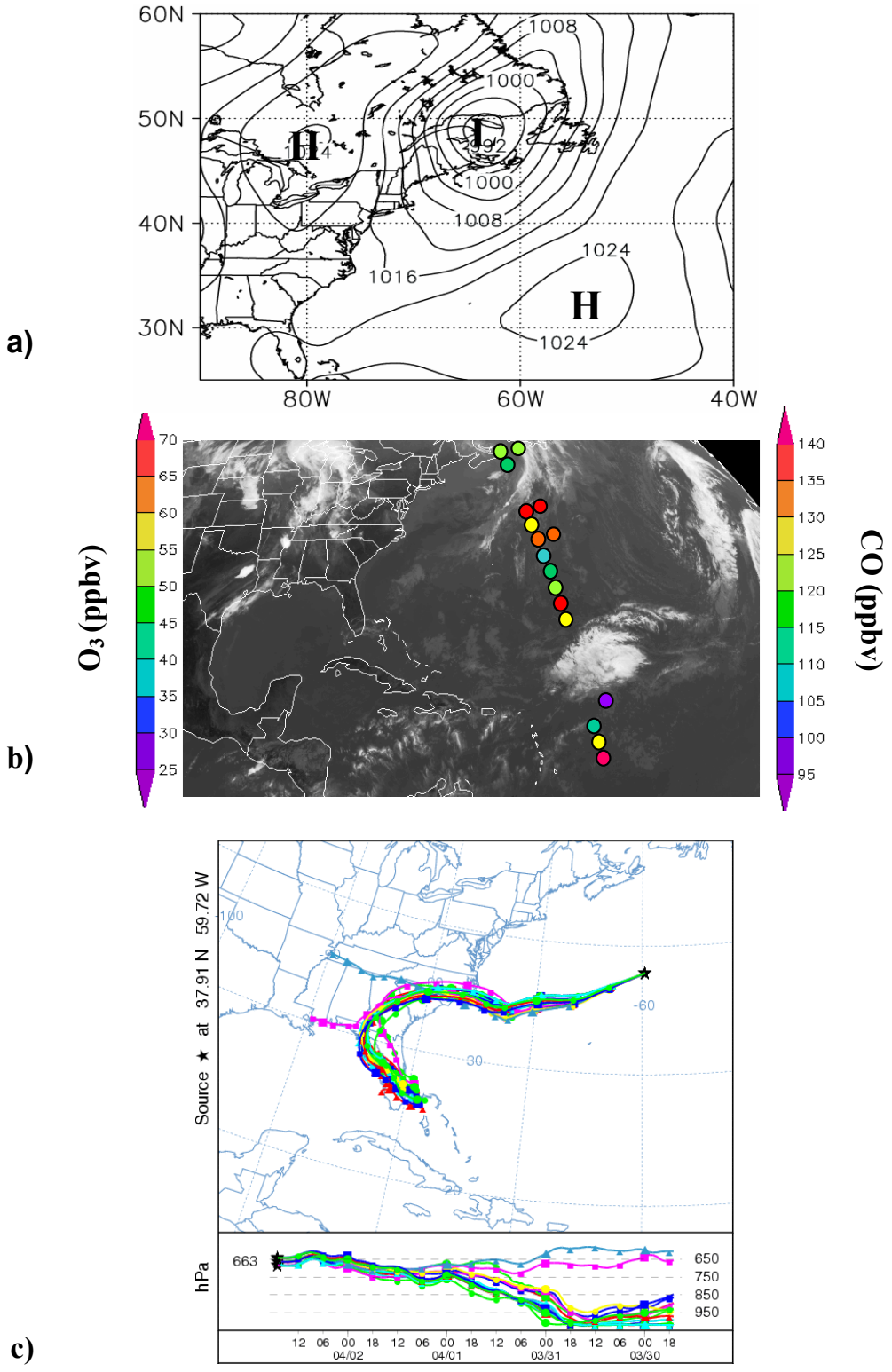


**Fig. 11. (a)** NCEP FNL SLP analysis for 12:00 UTC 2 April 2006 **(b)** GOES East IR image for 17:15 UTC 2 April 2006 with TES 681 hPa $O_3$ and CO (ppbv) retrievals plotted as colored dots at approximate ground footprint locations. The CO observations are offset slightly to the right from the actual locations and the dot sizes are not representative of the footprint sizes. **(c)** HYSPLIT ensemble back trajectories calculated using EDAS meteorological data for the corresponding time and location of the TES observations from 3500 m a.m.s.l.

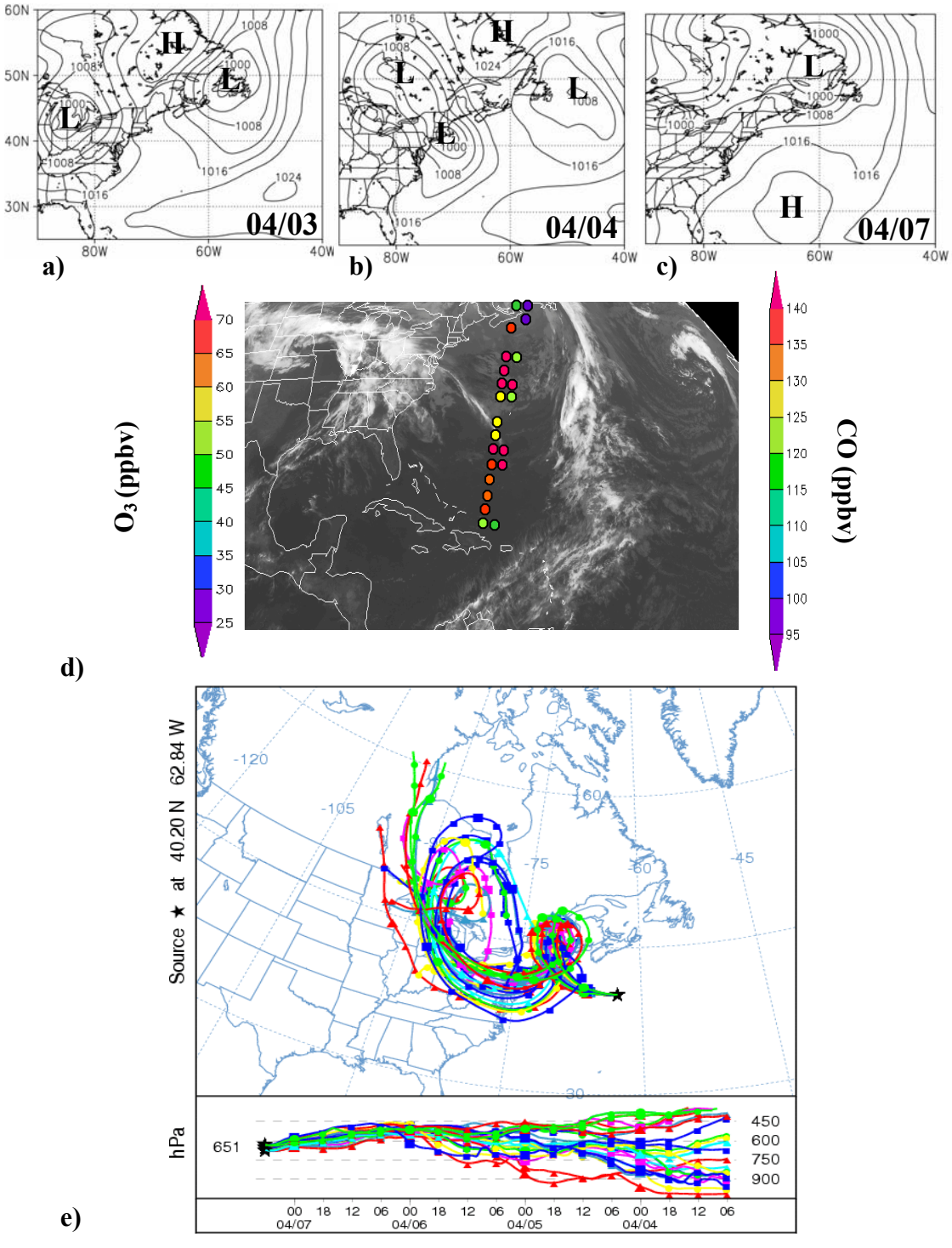


**Fig. 12.** NCEP FNL SLP analyses (hPa) for 12:00 UTC **(a)** 3 April, **(b)** 4 April, and **(c)** 7 April 2006 and **(d)** GOES East IR image for 07:15 UTC 7 April 2006 with TES 681 hPa $O_3$ and CO (ppbv) retrievals (offset slightly to the right) plotted for one orbit as colored dots at approximate ground footprint locations. HYSPLIT ensemble back trajectories **(e)** calculated using EDAS meteorological data for the corresponding time and location of TES observations from 3500 m a.m.s.l.

and eastward well out to sea produced large-scale subsidence conditions which were unfavorable for lofting pollutants into the lower free troposphere. The only area of enhanced 681 hPa $O_3$ in the western North Atlantic Ocean was near Newfoundland and was likely associated with stratospheric intrusions. This area featured enhanced 400 hPa PV (Fig. 3f) and a region of enhanced 316 hPa $O_3$ with levels exceeding 160 ppbv (Fig. 9f).

## 5 Export case studies

The composite figures of $O_3$ and CO include instantaneous measurements from different times and locations, whereas the map types reflect the average state of circulation patterns. Naturally it is difficult to make a direct link between the two when the temporal and spatial scales of a pollution event and a weather system are not directly comparable. There are indeed many details in $O_3$ and CO distributions that need to be interpreted using instantaneous measurements. We thus examined individual cases to determine the likely export pathways. Two examples discussed in this section illustrate how pollutants are transported from the continent to the lower free troposphere over the western Atlantic Ocean by cyclones under specific map type conditions. Both involve transport via the WCB but depict different locations for the $O_3$ enhancements with respect to the position of the cyclone.

The first example was a case of MAM2 on 2 April 2006 when high $O_3$ and CO at 681 hPa was measured by TES in the main branch of a WCB. On 31 March a compact surface low pressure system was located over the upper Midwest and a surface high pressure was located just off the South Carolina coast producing general southwesterly flow from the eastern Gulf of Mexico toward the northeastern states. The low pressure center tracked eastward and elongated in the north-south direction during the next two days while the high moved further off shore. By 12:00 UTC the surface low center was located over eastern Quebec with a sharp trough extending southward just off the east coast (Fig. 11a).

The TES retrieved 681 hPa $O_3$ exceeded 70 ppbv and 681 hPa CO exceeded 140 ppbv near the intersection of 40° N and 60° W during the afternoon ascending overpass (Fig. 11b). From the cloud pattern the high pollutant levels appeared to be in the WCB branch of the cyclonic system. On the northwestern side of the cloud band marking the WCB the $O_3$ level decreased to 45–50 ppbv and CO to ∼120 ppbv. An ensemble of backward trajectories using EDAS meteorological data (Fig. 11c) from near the locations of elevated $O_3$ and CO retrievals confirmed that these parcels were part of a slowly ascending airstream passing over the southeastern US boundary layer and eastern Gulf of Mexico during the previous 2–3 days where they potentially entrained anthropogenic pollutants.

The WCB is often an area of thick cloudiness obscuring satellite measurements of lower tropospheric $O_3$ and CO. For example, in Fig. 11b the orbit is clearly interrupted by the cloud band and resumes on the other side. However, this case demonstrated the ability of TES to measure at least some of the impact of WCB outflow on western Atlantic $O_3$ levels.

In the second example high $O_3$ and CO at 681 hPa occurred in mainly clear skies behind the main WCB region on 7 April 2006, a day also classified as MAM2 (Fig. 12). A low pressure center tracking into southern Canada from the Midwest on 3 April spawned a secondary development off the New York and New Jersey coast on 4 April (Fig. 12a and b). This new low center became the primary low as it tracked northeastward into the Canadian Maritimes on 7 April (Fig. 12c).

At approximately 06:00 UTC 7 April TES measured high 681 hPa $O_3$ (>70 ppbv) and CO (120–185 ppbv) on the descending Aura overpass which occurred just south of 40° N and near 63° W (Fig. 12d). An ensemble of HYSPLIT backward trajectories using EDAS meteorological data showed that air parcels passed over the urban areas of the northeastern US in the lower troposphere before ascending into the middle troposphere. In the meantime these air parcels moved northeastward into southeastern Canada then turned cyclonically to the west and eventually southeastward toward the ocean while descending back to the lower troposphere (Fig. 12e). Some of the ensemble members remained in the boundary layer over the east coast urban areas before being lofted into the mid-troposphere by the developing storm system on 4 April. These backward trajectories and coincident high CO and $O_3$ together suggest that the high mixing ratios behind or to the west of the storm center and main WCB were influenced by export of pollutants from the urban northeast corridor of the US.

This is an important finding because while Owen et al. (2006) report a case of high CO attributed to lofted continental pollutants that descended on the back side of a cyclone, generally high $O_3$ levels in the lower troposphere to the west of the surface low center have been linked to $O_3$-rich air descending from the upper troposphere or stratosphere in the DA (Cooper et al., 2001, 2002; Moody et al, 1996; Merrill et al., 1996; Oltmans et al., 1996). The trajectories of our case followed the same general track as the secondary WCB branch designated as W2 by Cooper et al. (2001), in which high $O_3$ levels were attributed to stratospheric air mixed into the polluted air of the WCB. However, since most of the back trajectories for our case remained in the lower or middle free troposphere and CO levels were high it is possible that a significant amount of the $O_3$ enhancement was due to anthropogenic contributions. Thus, this case suggests that the W2 branch may also be an important pollutant export stream capable of influencing the $O_3$ levels over the western North Atlantic Ocean.

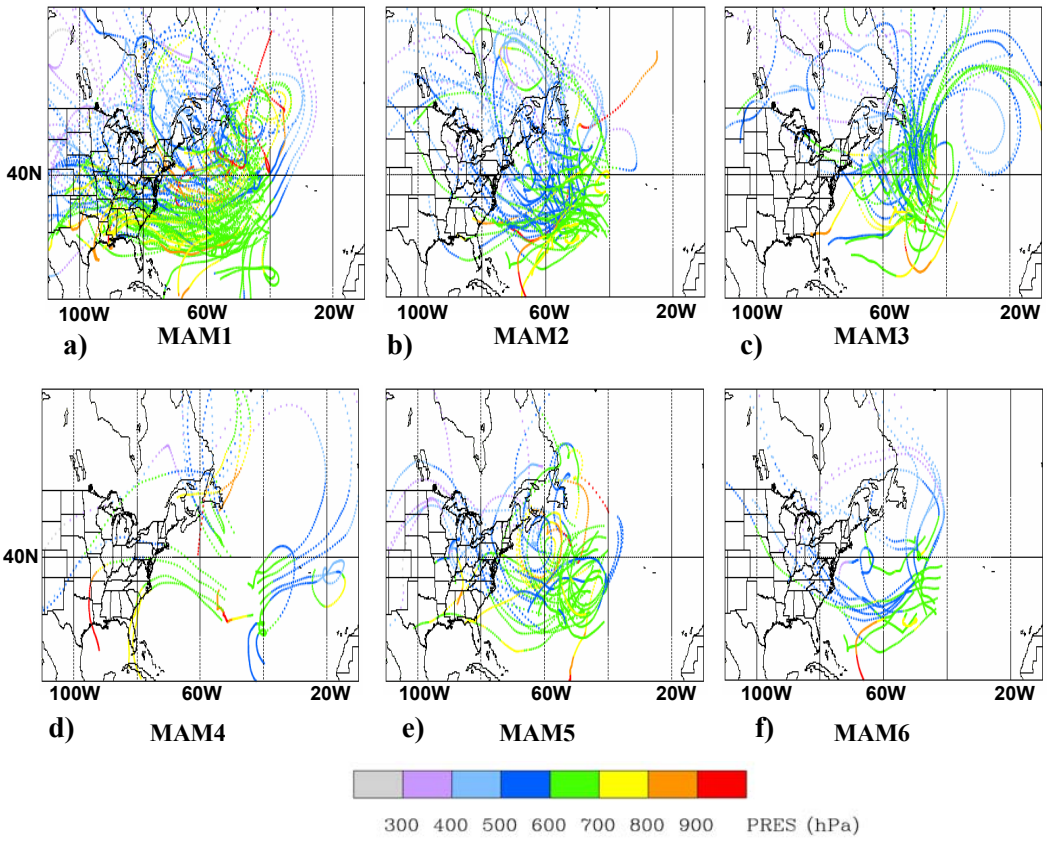


**Fig. 13.** Four-day HYSPLIT back trajectories using GDAS data from locations of TES 681 hPa observations in Region 3 for map types MAM1-MAM6 **(a–f)**. The colors indicate the pressure levels (hPa) of the trajectory parcels.

## 6 Evolution of continental outflow

Tying the $O_3$ and CO distributions in the central North Atlantic Ocean to the map types is challenging for a number of reasons. First, the map typing domain only extended eastward to 50° W and therefore the classification of the synoptic types did not directly consider the circulation dynamics in the center of the Atlantic Ocean. Second, the NCEP meteorological analyses used in map typing and trajectory calculations are based on fewer observations over the ocean and are therefore subject to greater errors. Third, the central North Atlantic Ocean is more distant from the sources of anthropogenic pollutants which allows for dilution and chemical transformation of exported plumes. Nevertheless, the TES composite distributions do show some interesting features which we discuss briefly in this section.

The polluted continental air in the free troposphere appeared to have been diluted as it was transported toward the central North Atlantic Ocean as the mixing ratios of CO at 681 hPa noticeably dropped off to below 120 ppbv east of 55° W (Fig. 4b). A few studies have presented global distributions of spring CO columns from AIRS, MOPITT and SCIAMACHY satellite instruments that show a similar decrease in CO levels away from the North American coastline (Buchwitz et al., 2007; Warner et al., 2007; Tangborn et al., 2009). In addition Edwards et al., 2004 showed this decrease was evident in AIRS and MOPITT 500 hPa distributions during the summer. However, unlike CO levels, the 681 hPa $O_3$ levels increased gradually from the US east coast until approximately 60° W and then leveled off and remained at almost the same levels across the Atlantic Ocean (Fig. 4a). In addition the seasonal mean $O_3$-CO slope increased to 0.17 mol mol$^{-1}$ in Region 3 from a value of 0.13 mol mol$^{-1}$ in Region 1 (Table 2), indicating more net $O_3$ increase and/or slower loss rate of $O_3$ than that of CO. As for Region 1, the slope in Region 3 was statistically significant at the $p$=0.01 level. This increase in slope in Region 3 was also evident in each of the most frequent map types MAM1-MAM3 as these ranged from 0.20–0.29 mol mol$^{-1}$ and were all statistically significant to at least the $p$=0.10 level (Table 2).

One possible explanation for the slower loss rate of $O_3$ compared to CO, which is consistent with the increased $O_3$-CO slopes, is that $O_3$ continued to be produced in the plume during transport (Mao et al., 2006). Summertime

observations at a mountain top site in the Azores have indicated $O_3$-CO slopes near 1.0 attributed to air masses in North American outflow events having undergone days of photochemical processing, producing the high $O_3$-CO slopes (Honrath et al., 2004). Another possible explanation for the slower decrease of $O_3$ level compared to CO is that contributions from the upper-level air transported downward in the descending DA of cyclones further east may have enhanced the lower tropospheric $O_3$ keeping levels high.

In terms of the map type composite distributions, the 681 hPa CO seemed to drop off more gradually toward the east in MAM1 than for the other map types (Fig. 6). The composite of GDAS 4-day back trajectories for Region 3, generated as in Fig. 7 by launching a single trajectory from each of the TES 681 hPa locations, indicated that this part of the central North Atlantic Ocean was significantly influenced by the eastern edge of the WCB extending from North America as the cyclones of MAM1 swept northeastward toward Newfoundland (Fig. 13). Interestingly, the WCB of MAM1 has a stronger influence in Region 3 than for Region 1 as discussed in Sect. 4 and this is due to the eastern location and large size of this low pressure system. For map types MAM2-MAM5, the trajectory composites showed a variety of pathways suggesting that pollutants exported from North America had been re-circulated and mixed with descending air from the upper troposphere and lower stratosphere diluting CO while keeping $O_3$ levels enhanced (Fig. 13b–e). The area of enhanced 681 hPa CO near the southeastern corner of the domain for MAM6 which resulted from just a small number of observations exceeding 140 ppbv seemed to be an anomalous feature that could not be traced back to any continental source using 4-day back trajectory analysis. Thus the actual source was likely very distant and the feature not representative of the expected CO concentrations for this circulation pattern. Overall there still seemed to be some connection between TES distributions in the central North Atlantic Ocean and the map types, particularly when comparing the CO distribution for MAM1 with those of the other map types, though clearly it was not as strong as for the regions closer to the North American coastline.

## 7 Summary

The springtime tropospheric $O_3$ and CO distributions constructed using the 2005 and 2006 TES measurements exhibited notable variability over 6 map types (MAM1-MAM6) representing the predominant circulation patterns over eastern North America and the western North Atlantic Ocean. The highest $O_3$ and CO levels in the lower free troposphere of the western North Atlantic Ocean were associated with map types MAM2-MAM3 featuring cyclones near the east coast of the US. We hypothesize that these elevated levels were due to lofting of anthropogenic pollutants from the continental boundary layer via the WCB of cyclones. Case studies for the cyclonic map type MAM2 demonstrated using back trajectories that retrievals of elevated 681 hPa $O_3$ and CO could be attributed to air parcels encountering the polluted continental boundary layer before being brought to the lower free troposphere by the WCB.

An important finding emerged from this study that boundary layer pollutants were exported to the lower free troposphere via a secondary branch (W2) circling around to the back of the cyclone center, in addition to the widely studied transport route facilitated by the main branch to the east of the cold front. This result suggested an additional mechanism for $O_3$ enhancement in the region which had been considered to be influenced mainly by stratospheric intrusions facilitated by the DA airstream. Also, since this region is typically clearer than the main WCB branch where clouds may obscure many of the TES measurements it is potentially an important region for studying North American export using satellites.

The TES $O_3$ composites also revealed evidence of stratospheric intrusions associated with the cyclones depicted in the map types. Overall, these features were most pronounced north of 45° N in the western North Atlantic Ocean. However, a complicating issue was that in these regions the averaging kernel tended to shift to higher altitudes and thus observed increases in the 681 hPa $O_3$ levels were partly due to the fact that the TES retrieval was weighted more toward the upper troposphere.

Composites of TES $O_3$ and CO retrievals showed the main export band extending from 30° N to 45° N with a seasonal $O_3$-CO slope of 0.13 mol mol$^{-1}$ at 681 hPa ranging up to 0.20 mol mol$^{-1}$ for the most favorable circulation patterns. The $O_3$-CO slopes derived from TES at 681 hPa were consistent with those derived from in situ measurements at ground sites and from aircraft in the lower free troposphere downwind of urban and industrial areas of North America (Parrish et al., 1993, 1998; Daum et al., 1996; Zhang et al., 2006) and were generally statistically significant at the $p$=0.10 level or better. Once over the ocean the pollutants became diluted as evident from the drop off in CO levels to the east of 55° W. However, $O_3$ levels continued to be elevated presumably due to photochemical production and in some cases transport of $O_3$ down from the upper troposphere in the DAs of cyclones further east.

There are limitations associated with using satellite retrievals to examine in detail the highly variable tropospheric $O_3$ distributions, namely the obscuring effects of clouds, the low vertical resolution (i.e. broad averaging kernel peaks), and lack of boundary layer sensitivity. However, the TES retrievals captured a high degree of variability with circulation patterns that was consistent with previous studies of North American export. Therefore, TES measurements incorporated into detailed observational and modeling systems should enable improvements to be made in the study of continental export.

*Acknowledgements.* The TES Level 2 data were obtained from the NASA Langley Research Center Atmospheric Sciences Data Center. Funding for this work was provided through the NASA Earth and Space Science Fellowship Program under grant NNG05GQ30H, the University of New Hampshire Space Grant Program under grant NNG05GG76H and by the Office of Oceanic and Atmospheric Research of the National Oceanic and Atmospheric Administration under AIRMAP grant NA06OAR4600189. The GOES satellite images were obtained from the data archive at the Plymouth State University Weather Center.

Edited by: O. Cooper

## References

Angevine, W. M., Senff, C., J., White, A. B., et al.: Coastal boundary layer influence on pollutant transport in New England, J. Appl. Meteorol., 43, 1425–1437, 2004.

Appenzeller, C., Davies, H. C., and Norton, W. A.: Fragmentation of stratospheric intrusions, J. Geophys. Res., 101, 1435–1456, 1996.

Auvray, M. and Bey, I.: Long-range transport to Europe: Seasonal variations and implications for the European ozone budget, J. Geophys. Res., 110, D11303, doi:10.1029/2004JD005503, 2005.

Auvray, M., Bey, I., Llull, E., Schultz, M. G., and Rast, S.: A model investigation of tropospheric ozone chemical tendencies in long-range transported pollution plumes, J. Geophys. Res., 112, D05304, doi:10.1029/2006JD007137 2007.

Banic, C. M., Leaitch, W. R., Isaac, G. A., Couture, M. D., Kleinman, L. I., Springston, S. R., and MacPherson, J. I.: Transport of ozone and sulfur to the North Atlantic atmosphere during the North Atlantic Regional Experiment, J. Geophys. Res., 101, 29091–29104, 1996.

Beer, R.: TES on the Aura Mission: Scientific objectives, measurements an analysis overview, IEEE T. Geosci. Remote Sens., 44(5), 1102–1105, 2006.

Beer, R., Glavich, T. A., and Rider, D. M.: Tropospheric Emission Spectrometer for the Earth Observing System's Aura satellite, Appl. Optics, 40, 2356–2367, 2001.

Bell, G. D. and Bosart, L. F.: A 15-year climatology of Northern Hemisphere closed cyclone and anticyclone centers, Mon. Weather Rev., 117, 2142–2163, 1989.

Berkowitz, C. M., Daum, P. H., Spicer, C. W., and Busness, K. M.: Synoptic patterns associated with the flux of excess ozone to the western North Atlantic, J. Geophys. Res., 101, 28923–28933, 1996.

Bowman, K. W., Rodgers, C. D. Kulawik, S. S., et al.: Tropospheric Emission Spectrometer Retrieval method and error analysis, IEEE T. Geosci. Remote Sens., 44(5), 1297–1307, 2006.

Bowman K. W., Worden, J., Steck, T.,Worden, H. M., Clough, S., and Rodgers, C. D.: Capturing time and vertical variability of tropospheric ozone: A study using TES nadir retrievals, J. Geophys. Res., 107, D23, 4723, doi:10.1029/2002JD002150, 2002.

Brasseur, G. P., Hauglustaine, D. A., Walters, S., et al.: MOZART: A global chemical transport model for ozone and related chemical tracers: 1. Model description, J. Geophys. Res., 103, 28265–28289, 1998.

Buchwitz, M., Khlystova, I., Bovensmann, H., and Burrows, J. P.: Three years of global carbon monoxide from SCIAMACHY: comparison with MOPITT and first results related to the detection of enhanced CO over cities, Atmos. Chem. Phys., 7, 2399–2411, 2007, http://www.atmos-chem-phys.net/7/2399/2007/.

Carlson, T. N.: Midlatitude Weather Systems, Am. Meteorol. Soc., Boston, 507 pp., 1998.

Chin, M., Jacob, D. J., Munger, J. W., Parrish, D. D., and Doddridge, B. G.: Relationship of ozone and carbon monoxide over North America, J. Geophys. Res., 99, 14565–14573, 1994.

Cooper, O. R., Moody, J. L., Parrish, D. D., et al.: Trace gas signatures of the airstreams within North Atlantic cyclones: Case studies from the North Atlantic Regional Experiment (NARE '97) aircraft intensive, J. Geophys. Res., 106, 5437–5456, 2001.

Cooper, O. R., Moody, J. L., Parrish, D. D., et al.: Trace gas composition of midlatitude cyclones over the western North Atlantic Ocean: A conceptual model, J. Geophys. Res., 107, D7, 4056, doi:10l1029/2001JD000901, 2002.

Cooper, O. R., Stohl, A., Eckhardt, S., et al.: A springtime comparison of tropospheric ozone and transport pathways on the east and west coasts of the United States, J. Geophys. Res., 110, D05S90, doi:10.1029/2004JD005183, 2005.

Crawford, J., Olson, J., Davis, D., Chen, G., et al.: Clouds and trace gas distributions during TRACE-P, J. Geophys. Res., 108, D21, 8818, doi:10.1029/2002JD003177, 2003.

Creilson, J. K., Fishman, J., and Wozniak, A. E.: Intercontinental transport of tropospheric ozone: A study of its seasonal variability across the North Atlantic utilizing tropospheric ozone residuals and its relationship to the North Atlantic Oscillation, Atmos. Chem. Phys., 3, 2053–2066, 2003, http://www.atmos-chem-phys.net/3/2053/2003/.

Daum, P. H., Kleinman, L. I., Newman, L., et al.: Chemical and physical properties of plumes of anthropogenic pollutants transported over the North Atlantic during the North Atlantic Regional Experiment, J. Geophys. Res., 101, 29029–29042, 1996.

Derber, J. C., Parrish, D. F., and Lord, S. J.: The new global operational analysis system at the National Meteorological Center, Weather Forecast., 6, 538–547, 1991.

Draxler, R. R. and Rolph, G. D.: HYSPLIT (HYbrid Single-Particle Lagrangian Integrated Trajectory) Model access via NOAA ARL READY, NOAA Air Resources Laboratory, Silver Spring, MD, 2003, http://www.arl.noaa.gov/ready/hysplit4.html .

Eckhardt, S., Stohl, A., James, P., Forster, C., and Spichtinger, N.: A 15-year climatology of warm conveyor belts, J. Climate, 17, 218–236, 2004.

Edwards, D. P., Emmons, L. K., Hauglustaine, D. A., Chus, D. A., et al.: Observations of carbon monoxide and aerosols from the Terra satellite: Northern Hemisphere variability, J. Geophys. Res., 109, D24202, doi:10.1029/2004JD004727, 2004.

Fehsenfeld, F. C., Ancellet, G., Bates, T. S., Goldstein, A. H., Hardesty, R. M., Honrath, R., et al.: International Consortium for Atmospheric Research on Transport and Transformation (ICARTT): North America to Europe – Overview of the 2004 summer field study, J. Geophys. Res., 111, D23S01, doi:10.1029/2006JD007829, 2006.

Fishman, J., Watson, C. E., Larsen, J. C., and Logan, J. A.: Distribution of tropospheric ozone determined from satellite data, J. Geophys. Res., 95, 3599–3617, 1990.

Fishman, J., Creilson, J. K., Wozniak, A. E., and Crutzen, P. J.: Interannual variability of stratospheric and tropospheric ozone determined from satellite measurements, J. Geophys. Res., 110,

D20306, doi:10.1029/2005JD005868, 2005.

Hegarty, J. D., Mao, H., and Talbot, R.: Synoptic controls on summertime surface ozone in the northeastern US, J. Geophys. Res., 112, D14306, doi:10.1029/2006JD008170, 2007.

Honrath, R. E., Owen, R. C., Val Martin, M., et al.: Regional and hemispheric impacts of anthropogenic and biomass burning emissions on summertime CO and $O_3$ in the North Atlantic lower free troposphere, J. Geophys. Res., 109, D24310, doi:10.1029/2004JD005147, 2004.

Huntrieser, H., Heland, J., Schlager, C., et al.: Intercontinental air pollution transport from North America to Europe: Experimental evidence from airborne measurements and surface observations, J. Geophys. Res., 110, D01305, doi:10.1029/2004JD005045, 2005.

Jacob, D. J., Logan, J. A., Gardner, G. M., Yevich, R. M., Spivakovsky, C. M., and Wofsy, S. C.: Factors regulating ozone over the United States and its export to the global atmosphere, J. Geophys. Res., 98, 14817–14826, 1993.

Kasibhatla, P., Levy II, H., Klonecki, A., and Chameidas, W. L.: Three-dimensional view of large-scale tropospheric distribution over the North Atlantic Ocean During Summer, J. Geophys. Res., 101, 29305–29316, 1996.

Key, J. R. and Chan, A. C. K.: Multidecadal global and regional trends in 1000 mb and 500 mb cyclone frequencies, Geophys. Res. Lett., 26, 2053–2056, 1999.

Kiley, C. M. and Fuelberg, H. E.: An examination of summertime cyclone transport during Intercontinental Chemical Transport Experiment (INTEX-A), J. Geophys. Res., 111, D25S06, doi:10.1029/2006JD007115, 2006.

Kim, S. W., Heckel, A., Mckeen, S. A., et al.: Satellite-observed US power plant NOx emission reductions and their impact on air quality, Geophys. Res. Lett., 33, L22812, doi:10.1029/2006GL027749, 2006.

Kim, S. Y., Talbot, R., Mao, H., et al.: Continental outflow from the US to the upper troposphere over the North Atlantic during the NASA INTEX-NA Airborne Campaign, Atmos. Chem. Phys., 8, 1989–2005, 2008, http://www.atmos-chem-phys.net/8/1989/2008/.

Kulawik, S. S., Worden, J., Eldering, A., et al.: Implementation of cloud retrievals for Tropospheric Emission Spectrometer (TES) atmospheric retrievals: 1. Description and characterization of errors on trace gas retrievals, J. Geophys. Res., 111, D24204, doi:10.1029/2005JD006733, 2006.

Lamaraque, J. F., Langford, A. O., and Proffitt, M. H.: Cross-tropopause mixing of ozone through gravity wave breaking: Observation and modeling, J. Geophys. Res., 101, 22969–22976, 1996.

Li, Q., Jacob, D. J., Rokjin, P., et al.: North American pollution outflow and the trapping of convectively lifted pollution by upper-level anticyclone, J. Geophys. Res., 110, D10301, doi:10.1029/2004JD005039, 2005.

Luo, M., Beer, R., Jacob, D. J., et al.: Simulated observation of tropospheric ozone and CO with Tropospheric Emission Spectrometer (TES) satellite instrument, J. Geophys. Res., 107, D15, doi:10.1029/2001JD000804, 2002.

Lund, I. A.: Map-pattern classification by statistical methods, J. Appl. Meterorol., 2, 56–65, 1963.

Mao, H. and Talbot, R.: $O_3$ and CO in New England: Temporal variations and relationships, J. Geophys., Res., 109, D21304, doi:10.1029/2004JD004913, 2004.

Mao, H., Talbot, R., Troop, D., Johnson, R., Businger, S., and Thompson, A. M.: Smart balloon observations over the North Atlantic: $O_3$ data analysis and modeling, J. Geophys. Res., 111, D23S56, doi:10.1029/2005JD006507, 2006.

Merrill, J. T., Moody, J. L., Oltmans, S. J., and Levy, H. II: Meteorological analysis of tropospheric ozone profiles at Bermuda, J. Geophys. Res., 101, 29201–29211, 1996.

Moody, J. L., Davenport, J. C., Merrill, J. T., et al.: Meteorological mechanisms for transporting $O_3$ over the western North Atlantic Ocean: A case study for 24–29 August 1993, J. Geophys. Res., 101, 29213–29277, 1996.

Monks, P. S.: A review of the observations and origins of the spring ozone maximum, Atmos. Environ., 34, 3545–3561, 2000.

Nassar R., Logan, J. A., Worden, H. M., et al.: Validation of Tropospheric Emission Spectrometer (TES) nadir ozone profiles using ozonesonde measurements, J. Geophys. Res., 113, D15S17, doi:10.1029/2007JD008819, 2008.

Oltmans, S. J., Levy II, H., Harris, J. M., et al.: Summer and spring ozone profiles over the North Atlantic from ozonesonde measurements, J. Geophys. Res., 101, 29179–29200, 1996.

Osterman, G., Bowman, K., Cady-Pereira, K., et al.: Tropospheric Emission Spectrometer (TES), validation report, JPL D#102, version 2.0, http://eosweb.larc.nasa.gov/PRODOCS/tes/validation/TESValidationReport_v2_0.pdf, 2007a.

Osterman G., Bowman K. W., Eldering, A., Fisher, B., et al.: TES Level 2 (L2) Data User's Guide, Version 3.0, Jet Propulsion Laboratory, Pasadena, CA, http://tes.jpl.nasa.gov/uploadedfiles/TES_L2_Data_Users_Guide-1.pdf, 2007b.

Owen, R. C., Cooper, O. R., Stohl, A., and Honrath, R. E. : An analysis of the mechanisms of North American pollutant transport to the central North Atlantic lower free troposphere, J. Geophys. Res., 111, D23S58, doi:10.1029/2006JD007062, 2006.

Parrish, D. D., Holloway, J. S., Trainer, M., et al.: Export of North American ozone pollution to the North Atlantic Ocean, Science, 259, 1436–1439, 1993.

Parrish, D. D., Trainer, M., Holloway, J. S., et al.: Relationships between ozone and carbon monoxide at surface sites in the North Atlantic region, J. Geophys. Res., 103, 13357–13376, 1998.

Parrish, D. D., Holloway, J. S., Jakoubek, R., et al.: Mixing of anthropogenic pollution with stratospheric ozone: A case study from the North Atlantic wintertime troposphere, J. Geophys. Res., 105, 24363–24374, 2000.

Polvani, L. M. and Esler, J. G.: Transport and mixing of chemical air masses in idealized baroclinic life cycles, J. Geophys., Res. 112, D23102, doi:10.1029/2007JD008555, 2007.

Rodgers, C. D.: Inverse Methods for Atmospheric Sounding: Theory and Practice, World Sci., Hackensack, N. J, 2000.

Rodrigues, S., Torres, C., Guerra, J.-C., and Cuevas, E.: Transport pathways of ozone to marine and free-troposphere sites in Tenerife, Canary Islands, Atmos. Environ., 38, 4733–4747, 2004.

Schoeberl, M. R.: Overview of the EOS Aura mission, IEEE T. Geosci. Remote Sens., 44, 5, 1066–1074, 2006.

Serreze, M. C., Carse, F., Barry, R. G., and Rogers, J. C.: Icelandic Low Cyclone Activity: Climatological Features, Linkages with the NAO, and Relationships with Recent Changes in the Northern Hemisphere Circulation, J. Climate, 10, 453–464, 1997.

Shapiro, M. A., Hampel, T., and A. J. Krueger: The arctic tropopause fold, Mon. Weather Rev., 115, 444–454, 1987.

Shim, C., Li, Q., Luo, M., Kulawik, S., Worden, H., Worden, J., Eldering, A., Diskin, G., Sachse, G., Weinheimer, A., Knapp, D., Montzca, D., and Campos, T.: Characterizing mega-city pollution with TES $O_3$ and CO measurements, Atmos. Chem. Phys. Discuss., 7, 15189–15212, 2007, http://www.atmos-chem-phys-discuss.net/7/15189/2007/.

Singh, H. B., Brune, W. H., Crawford, J. H., Jacob, D. J., and P. B. Russell: Overview of the summer 2004 International Chemical Transport Experiment- North America (INTEX-A), J. Geophys. Res., 111, D23S02, doi:10.1029/2006JD007905, 2006.

Stohl, A. M. and Trickl, T.: A textbook example of long-range transport: Simultaneos observation of ozone maxima of stratospheric North American origin in the free troposphere over Europe, J. Geophys. Res., 104, 30445–30462, 1999.

Stohl, A., Huntrieser, H., Richter, A., Beirle, S., Cooper, O. R., Eckhardt, S., Forster, C., James, P., Spichtinger, N., Wenig, M., Wagner, T., Burrows, J. P., and Platt, U.: Rapid intercontinental air pollution transport associated with a meteorological bomb, Atmos. Chem. Phys., 3, 969–985, 2003a, http://www.atmos-chem-phys.net/3/969/2003/.

Stohl, A., Forster, C., Eckhardt, S., et al.: A backward modeling study of intercontinental transport using aircraft measurements, J. Geophys. Res., 108, D12, 4370, doi:10.1029/2002JD002862, 2003b.

Tangborn, A., Stajner, I., Buchwitz, M., Khlystova, I., et al.: Assimilation of SCIAMACHY total column CO observations: Global and regional analysis of data impact, J. Geophys. Res., 114, D07307, doi:10.1029/2008JD010781, 2009.

Trickl, T., Cooper, O. R., Holger, E., et al.: Intercontinental transport and its influence on the ozone concentrations over Europe: Three case studies, J. Geophys. Res., 108, D12, 8530, doi:10.1029/2002JD002735, 2003.

Warner, J., Comer, M. M., Barnet, C. D., Mcmillan, W. W., et al.: A comparison of satellite tropospheric carbon monoxide measurements from AIRS and MOPITT during INTEX-A, J. Geophys. Res., 112, D12S17, doi:10.1029/2006JD00792, 2007.

Worden, H. M., Logan, J. A., Worden, J. R., et al.: Comparisons of Tropospheric Emission Spectrometer (TES) ozone profiles to ozonesondes: Methods and initial results, J. Geophys. Res., 112, D03309, doi:10.1029/2006JD007258, 2007.

Worden, J., Kulawik, S. S., Shephard, M. W., et al.: Predicted errors of Tropospheric Emission Spectrometer nadir retrievals from spectral window selection, J. Geophys. Res., 109, D09308, doi:10.1029/2004JD004522, 2004.

Worden, J., Liu, X., Bowman, K., et al.: Improved tropospheric ozone profile retrievals using OMI and TES radiances, Geophys. Res. Lett., 34, L01809, doi:10.1029/2006GL027806, 2007.

Zhang, L., Jacob, D. J., Bowman, K. W., et al.: Ozone-CO correlations determined by the TES satellite instrument in continental outflow regions, and prospects in synoptic climatology, Geophys. Res. Lett., 33, L18804, doi:10.1029/2006GL026399, 2006.

Zishka, K. M. and Smith, P. J.: The climatology of cyclones and anticyclones over North America and surrounding ocean environs for January and July, 1950–1977, Mon. Weather Rev., 108, 387–401, 1980.